MARMARA UNIVERSITY
INSTITUTE FOR GRADUATE STUDIES
IN PURE AND APPLIED SCIENCES

INVESTIGATION OF O-RING SEAL BEHAVIOR IN GASOLINE INJECTORS UNDER DIFFERENT FUELS AND OPTIMIZATION OF INJECTOR HYDRAULIC CONNECTION

H. GÖKBERK TARÇIN

MASTER THESIS

Department of Mechanical Engineering

Thesis Supervisor

Prof. Dr. Cenk SAYIN

ISTANBUL, 2024

MARMARA ÜNİVERSİTESİ
FEN BİLİMLERİ ENSTİTÜSÜ

BENZİNLİ ENJEKTÖRLERDEKİ SIZDIRMAZLIK PARÇASI O-RİNGİN FARKLI YAKITLAR ALTINDAKİ DAVRANIŞLARININ İNCELENMESİ VE ENJEKTÖR HİDROLİK BAĞLANTISININ OPTİMİZASYONU

H. GÖKBERK TARÇIN

YÜKSEK LİSANS TEZİ

Makine Mühendisliği Fakültesi

DANIŞMAN

Prof. Dr. Cenk SAYIN

İSTANBUL, 2024

TABLE OF CONTENTS

ABSTRACT I

ÖZET III

ORIGINALITY OF STUDY V

PREFACE- ACKNOWLEDGMENT V

SYMBOLS VI

ABBREVIATIONS VII

LIST OF FIGURES VIII

LIST OF TABLES IX

1. INTRODUCTION 1

  1.1. Alternative Fuels 2

  1.2. Fuel Injection Systems 4

    1.2.1. Port Fuel Injection (PFI) 4

    1.2.2. Gasoline Direct Injection (GDI) 5

  1.3. The Importance of O-Rings in Fuel Injectors 6

    1.3.1. Material Properties and Molecular Geometries of FKM 7

  1.4. O-Ring Vulnerability to Fuel Type 9

    1.4.1. Hardness 10

    1.4.2. Tensile Strength 11

    1.4.3. Elongation 11

  1.5. Hydraulic Interface and Importance of its Optimization 12

2. MATERIAL AND METHODS 14

    2.1.1. Real-world Applications 14

    2.1.2. Standardization and Comparability 14

    2.1.3. Material Properties Focus 15

    2.1.4. Accessibility and Availability Considerations 15

  2.2. Media Used in Testing and Immersion Test Followed by Drying 15

2.2.1. Gasoline Types 16

2.2.2. Procedure of Immersion Test and Drying 17

2.2.3. Phase Separation Behavior in Gasoline-Ethanol Blends 17

2.2.4. Test Equipment for Immersion Tests: 18

2.2.5. Machine for Drying O-rings 19

2.3. Hardness Test 21

2.3.1. Determination of Hardness Method 21

2.3.2. IRHD Measurement Device 22

2.3.3. Steps of IRHD Testing 23

2.4. Tensile Strength Test 23

2.4.1. Tensile Strength Machine and Fixture 24

2.4.2. Tensile Strength Test Procedure 26

2.5. Optimization of Hydraulic Connection 28

2.5.1. Parametric Study of FKM O-ring Dimensions and Piston Diameter 28

2.5.2. Influence of O-ring Hardness on Sealing Performance 32

3. RESULTS AND DISCUSSIONS 33

3.1. Media Immersion and Impact on O-ring 33

3.2. Numerical Analysis 38

4. CONCLUSION 49

REFERENCES 51

RÉSUMÉ 55

ABSTRACT

INVESTIGATION OF O-RING SEAL BEHAVIOR IN GASOLINE INJECTORS UNDER DIFFERENT FUELS AND OPTIMIZATION OF INJECTOR HYDRAULIC CONNECTION

In gasoline vehicles, the fuel pressurized in the pump is carried to the injectors with the rail and the injector keeps the fuel it receives inside the cylinder block at the desired angle. This phenomenon is called direct injection. In these systems where the injector is located, the tightness of the fuel and hot air gases plays a major role in terms of function and safety. The connection between the injector and the rail where the tightness is seen is used by several different methods in the industry, and the most common techniques among these are rubber O-rings and threaded apparatuses. The use of rubber-based O-rings in the automotive industry is regulated by DIN, ISO and EN standards. The surface geometries and O-ring materials on which the parts can be used are also specified in these standards. However, the determination of these values directly depends on private institutions.

Due to the differences between the fuel standards of the countries, the fuels that the O-rings are exposed to vary. However, the wear rates of the fuels vary within themselves and their effects on the O-rings are also different. In this thesis, the behavior of gasoline injector O-rings under fuels with different abrasion values will be examined by experimental fuel tests, and the wear correlation between O-ring and fuel will be determined through volumetric, hardness and strength changes. In order for the test results to be comparable, the O-ring material and geometry will be accepted as the whole singular value, while other parameters will vary.

O-rings with round cross-sectional area are mostly used in the industry, and the geometry where the part will be kept is adjusted to suit the radial insulation configuration, and this area where the insulation is made is called the hydraulic connection. In this configuration, the geometric parameters determine how much the pressed O-ring will swell. If the part does not swell enough after pressing, the sealing function cannot be fulfilled, which causes fuel leakage and pressure drop in the system.

While the fact that the fuel does not leak in the hydraulic connection is taken as a basis, the assembly, materials, weight, and price of the parts are also the values that are taken into consideration. In this sense, in the thesis, it is aimed to create different configurations of the hydraulic connection in accordance with the ISO 3601 standard by mathematical modeling and to present the optimal configuration.

The output of the studies aims to provide a guide for the sealing function of gasoline injectors used and to be used in the industry, and to provide a content that will be useful in determining the conditions of use of the existing parts.

ÖZET

BENZİNLİ ENJEKTÖRLERDEKİ SIZDIRMAZLIK PARÇASI O-RİNGİN FARKLI YAKITLAR ALTINDAKİ DAVRANIŞLARININ İNCELENMESİ VE ENJEKTÖR HİDROLİK BAĞLANTISININ OPTİMİZASYONU

Benzinli taşıtlarda pompada basınçlanan yakıt ortak yakıt borusu ile enjektörlere taşınmaktadır ve enjektör aldığı yakıtı dilenen açı ile silindir bloğunun içerisine muhafaza etmektedir. Bu olgu doğrudan püskürtme olarak adlandırılmaktadır. Enjektörün yer aldığı bu sistemlerde yakıtın ve sıcak hava gazlarının sızdırmazlığı fonksiyon ve güvenlik açısından büyük rol oynamaktadır. Sızdırmazlığın görüldüğü enjektör-ortak yakıt borusu arasındaki bağlantı, endüstride birkaç farklı yöntem ile kullanılmaktadır ve bunlar arasındaki en yaygın teknikler kauçuk O-ringler ve vidalı dişi olan aparatlardır. Otomotiv sektöründe kauçuk bazlı O-ringlerin kullanımı DIN, ISO ve EN standartları ile kurallandırılmıştır. Parçaların kullanılabileceği yüzey geometrileri ve O-ring materyalleri de bu standartlarda belirtilmektedir. Fakat bu değerlerin belirlenmesi doğrudan özel kurumlara bağlıdır.

Ülkelerin yakıt standartları arasındaki farklılıklardan dolayı O-ringlerin maruz kaldığı yakıtlar çeşitlilik göstermektedir. Fakat, yakıtların aşındırma oranları kendi içinde değiştiği gibi O-ringler üzerindeki etkileri de farklıdır. Bu tezde benzinli enjektör O-ringlerinin farklı aşındırma değerlerine sahip yakıtlar altındaki davranışları deneysel yakıt testleri ile incelenip, O-ring – yakıt arasındaki aşınma korelasyonu hacimsel, sertlik ve mukavemet değişimleri üzerinden saptanacaktır. Yapılan deney sonuçlarının kıyaslanabilir olması için O-ring malzemesi ve geometrisi bütün tekil değer kabul edilirken, diğer parametreler değişkenlik gösterecektir.

Endüstride çoğunlukla yuvarlak kesit alanına sahip O-ringler kullanılmaktadır ve parçanın muhafaza edileceği geometri, radyal izolasyon konfigürasyonun uygun olacak şekilde ayarlanmaktadır ve izolasyonun yapıldığı bu bölge hidrolik bağlantı olarak adlandırılmaktadır. Bu konfigürasyon içerisinde geometrik parametreler, preslenen O-ringin ne kadar şişeceğini belirlemektedir. Preslemeden sonra parça yeterince şişmez ise sızdırmazlık görevi yerine getirilemez, bu da sistemde yakıt kaçağına ve basıncın düşmesine sebep olur.

Hidrolik bağlantıda yakıtın sızmayacak şekilde olması başta esas alınırken, parçaların montajı, malzemeleri, ağırlığı ve fiyatı da dikkat edilen değerlerdir. Bu anlamda tez

içerisinde hidrolik bağlantının ISO 3601 standardına uygun olacak şekilde farklı konfigürasyonları matematiksel modelleme ile oluşturulup optimal konfigürasyonun sunulması hedeflenmektedir.

Yapılan çalışmaların çıktısı, endüstride kullanılan ve kullanılacak benzinli enjektörlerin sızdırmazlık fonksiyonu için hem yol gösterici hem de mevcuttaki parçaların kullanım koşullarının belirlenmesinde fayda sağlayacak bir içerik sunmayı hedeflemektedir.

ORIGINALITY OF STUDY

In order for O-rings to be used as fuel leakage preventing component, they need to meet certain criteria for automotive industry. Vehicle manufacturers require certain specifications on O-rings, such as elongation at break and tensile strength in original state, same values after fuel immersion, and so on. When the part does not meet any of the specified limits, vehicle manufacturers do not accept the component material and therefore the material of O-rings must be updated. Such cases set projects back to their initial state because an update in material change alters every behavior of the O-ring. These processes take an enormous amount of time and money, and there is no way to make sure that part will be okay, until it is tested. Even though some studies have been done on O-ring and fluid, such as aromatic compounds, in the past, results do not solely show the effect of gasoline-ethanol blends on elastomer O-rings. With the results that will be obtained in this thesis, it is aimed to create a reference for O-ring development by finding a relation between O-ring and gasoline-ethanol blends. This reference will solve the issue for exceeded project time plans on O-ring development and decrease the money spent. Additionally, studying mathematical models for new hydraulic connection will provide an optimized interface, which will decrease the fuel leakage incidents that occur at field.

PREFACE- ACKNOWLEDGMENT

The behavior of O-rings, such as deterioration, hardness, and tensile strength, varies under different fuels. Although there have been some studies focusing on O-ring behavior under different fuels in the past, there has been no study showing the relationship between the ethanol level of fuel and O-rings after aging. Therefore, one goal of this thesis is to find such a relationship by analyzing O-rings immersed in different types of fuels in terms of hardness, tensile strength, and volume changes. Thus, a contribution would be made to the literature, industry, and researchers working in this field.

During the preparation of this study, I would like to extend my gratitude to my thesis advisor, Prof. Dr. Cenk Sayın, for his extensive tolerance, experience, and invaluable support with his ideas. I also express my gratitude to my precious family, who has supported me with patience and love in every aspect throughout my life and education.

SYMBOLS

A_0	: Initial Cross Section Area of O-Ring
$A_{contact}$	: Contact Area Between O-Ring and Shaft
b_1	: Width of Groove
C	: Compression Percentage
d_1	: Inner Diameter of O-ring
d_2	: Cross Section Diameter of O-ring
d_3	: Piston Groove Diameter
d_4	: Shaft Diameter
d_9	: Seat Diameter
F	: Applied Force
F_{axial}	: Axial Force Applied by O-ring
F_{max}	: Maximum Force at Tear In N
G_{fill}	: Groove Fill Percentage
L_0	: Length of O-ring at Initial (Unstretched) Condition in mm
L_R	: Length of O-ring at Break in mm
mm	: Millimeter
N	: Newton
R	: Diameter Stretch
$S_{initial}$	: Stretch Percentage
V_{groove}	: Groove Volume
$V_{O\text{-}ring}$	: O-ring Volume
°C	: Degree Celsius
σ_{max}	: Tensile Strength at Break in N/mm

ABBREVIATIONS

CO_2	: Carbon Dioxide
FKM	: Fluorine Kautschuk Material
GDI	: Gasoline Direct Injection
HDEV	: High-Pressure Injector
ID	: Inner Diameter of O-Ring
IRHD	: International Rubber Hardness Degree
ISO	: International Organization for Standardization
OD	: Outer Diameter of O-ring
PFI	: Port Fuel Injection
TW-S	: Temperature wave shock
VW TL5266	: FKM-Elastomer for Gasoline Fuel Inserts in High-Pressure Injection Systems

LIST OF FIGURES

Figure 1.1 Regulated Gaseous Emissions from Gasoline and Gasohol Fueled Engines at Different Engine Loads 1
Figure 1.2 Gasoline Injection System........ 4
Figure 1.3 Comparison of the PFI and GDI Mixture Preparation Systems........ 5
Figure 1.4 Monomers That Synthesis FKM 8
Figure 1.5 Molecular Structure of FKM........ 8
Figure 2.1 O-ring Dimensions and Its Cross-Section View 14
Figure 2.2 Worldwide Used Gasoline Blends 16
Figure 2.3 Glass Bottle Setup for Immersion Tests........ 19
Figure 2.4 Vötsch VT3 7012 S2 Drying Machine........ 20
Figure 2.5 Types of Hardness Indenters 1) Conical 2) Spherical 3) Truncated Cone........ 21
Figure 2.6 Bareiss IRHD Compact III Machine 22
Figure 2.7 Zwick Roell Zwickline Z2.5 and Software 25
Figure 2.8 a) O-ring Mount Fixture, b) O-ring Mounted on the Fixture 26
Figure 2.9 O-ring Tensile Strength Test Setup; Initial Step Is Shown at Left Hand Side, Whereas Final Step Is Shown On Right 27
Figure 2.10 Radial Piston Seal Design 29
Figure 3.1 Volume Change of O-Rings Tested in Immersion Test........ 35
Figure 3.2 Boxplot of O-ring Tensile Strength........ 37
Figure 3.3 Boxplot of O-ring Elongation at Break Values........ 37
Figure 3.4 Effect of O-ring’s Inner Diameter on a) Initial Stretch, b) Compression, c) Initial Stretch and Compression 39
Figure 3.5 Effect of O-ring’s Cross Section Diameter On a) Compression, b) Groove Fill, c) Compression and Groove Fill........ 41
Figure 3.6 Effect of Piston Diameter On a) Initial Stretch, b) Compression, c) Groove Fill 43
Figure 3.7 Comparison of Dimension Contribution to Sealing Properties........ 43
Figure 3.8 Stress vs Strain of Non-immersed O-rings........ 44
Figure 3.9 Force and Pressure Comparison of Parametric Dimensions 45
Figure 3.10 Combined Analysis a) Dimensions, b) Seal Design Properties, c) Groove Fill and Compression Relation........ 47

LIST OF TABLES

Table 2.1 Gasoline-Ethanol Blends for Testing 16
Table 2.2 Specifications of Vötsch VT3 7012 S2 Drying Machine 20
Table 2.3 IRHD Compact III Technical Properties 22
Table 2.4 Properties of Zwick Roell Zwickline Z2.5 24
Table 2.5 Initial Dimension for Hydraulic Interface Optimization Study 29
Table 3.1 Initially Measured Dimensions and Hardness on O-rings 33
Table 3.2 Measured Dimensions and Hardness on O-rings After Immersion 34
Table 3.3 Volumetric Change Limit Comparison for E85 Immersion 36
Table 3.4 Change in O-Ring Volume After Immersion Test 36
Table 3.5 Change in O-ring IRHD After Immersion Test 36
Table 3.6 Acting Force and Pressure on Min and Max Dimensions 47
Table 3.7 Elastic Modulus at 100% Elongation of O-rings After Immersion 48
Table 3.8 Comparison of Immersed O-rings Properties 48

1. INTRODUCTION

Throughout the past century, internal combustion engines emerged as the preferred technology for both transportation and decentralized power generation. Over this extended period, these engines have consistently upheld their crucial position as the primary driving force behind global mobility, enabling billions of people worldwide to travel [1]. Within the complex structure of engine parts, fuel injectors stand out as essential components, tasked with ensuring not just the smooth functioning of engines, but also the efficient use of fuel and control of emissions [2]. Functioning as accurate distributors, fuel injectors are responsible for delivering carefully measured amounts of fuel into the combustion chamber, where it combines with surrounding air before igniting to propel the vehicle. The effectiveness and dependability of this complex process have significant implications for the overall performance and environmental impact of contemporary vehicles.

In recent years, there has been a significant shift in passenger vehicle fueling away from gasoline, driven by environmental concerns and the need to reduce reliance on fossil fuels. Ethanol emerges as a promising alternative, derived from renewable biomass sources, offering benefits like reduced greenhouse gas emissions and decreased dependence on non-renewable fuels. However, transitioning to ethanol presents challenges, especially in fuel injector design and performance optimization [3] (see Figure 1.1. [4]).

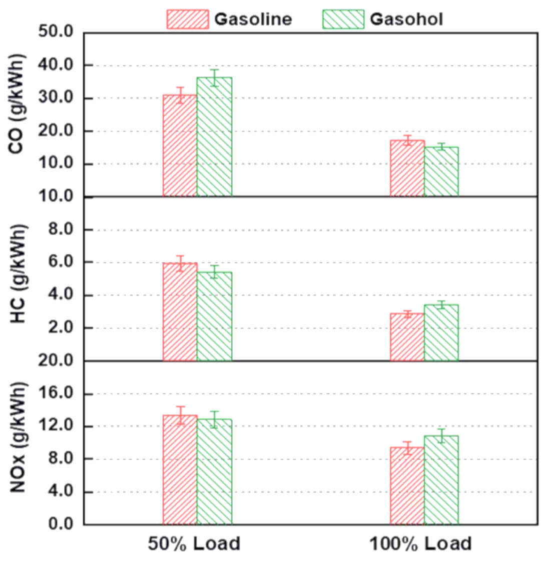

Figure 1.1 Regulated Gaseous Emissions from Gasoline and Gasohol Fueled Engines at Different Engine Loads

Transitioning to ethanol-based fuels requires redesigning fuel injectors to suit ethanol's distinct properties and combustion traits. Differences in viscosity, vapor pressures, and octane ratings call for customized engineering approaches to enhance fuel atomization, distribution, and combustion efficiency. In engines using ethanol port fuel injection, fuel spray characteristics vary with factors such as flow rate, injection duration, and ambient air crossflow, with shorter injections correlating with higher evaporation rates near the nozzle. Furthermore, the increasing use of ethanol-based fuels means that engine management systems must be adjusted to meet the specific fueling needs and combustion behaviors of ethanol [5], [6].

Given these factors, the intersection of automotive engineering and materials science becomes increasingly important, leading to the creation of new technologies that emphasize durability, effectiveness, and suitability for ethanol-based fuels. This quest for advancements not only offers potential for improving the performance and sustainability of current vehicles but also highlights the significant role of fuel injectors in guiding the direction of automotive propulsion towards a greener and more sustainable path [7].

Investigating Fuel injector O-rings is essential for the suggested design modifications, given their critical role in engine performance. The quality of these seals directly affects how well the engine operates. Any deficiencies, such as incorrect coloring or cuts, can cause substantial problems with the engine. Dhawale and his colleagues highlight that such imperfections in O-rings can lead to engine issues, underscoring the necessity for comprehensive research in this domain. It's crucial to ensure the reliability of Fuel injector O-rings to prevent potential engine failures and maintain optimal functioning [8].

As the automotive industry advances towards ethanol-based fuels, understanding the compatibility of O-ring materials becomes paramount. Bio-fuels distinct chemical properties necessitate careful selection of materials to mitigate risks of degradation and ensure long-term sealing effectiveness.

1.1. Alternative Fuels

The need for adopting alternative fuels arises from persistent challenges faced by transportation energy systems, such as climate change, urban air pollution, energy security issues, limited oil resources, and increasing demand for transportation services. While making vehicles more fuel-efficient is effective in addressing these challenges, its long-term impact is limited by projected future demand. Therefore, integrating alternative fuels like liquid biofuels, synfuels, hydrogen, and electricity becomes crucial for comprehensively tackling societal, environmental, and economic objectives within the transportation sector [9].

Several critical factors underscore this importance. Firstly, alternative fuels provide a means to diversify energy sources, reducing reliance on finite and geopolitically sensitive oil reserves. Secondly, they offer environmental benefits by producing lower greenhouse gas emissions and pollutants compared to conventional fossil fuels, contributing to a cleaner and more sustainable environment. Thirdly, alternative fuels offer a sustained solution, addressing the limitations of solely improving vehicle fuel efficiency. Additionally, they play a significant role in reducing dependence on automobiles, especially in countries where personal vehicle use is deeply ingrained. Overcoming barriers to the adoption of alternative fuel vehicles, including the lack of refueling infrastructure, is crucial for successfully introducing these vehicles. Economic considerations, along with the pivotal role of refueling availability, highlight the strategic importance of alternative fuels. In this context, integrating alternative fuels becomes not only an environmental imperative but also a practical step towards ensuring a resilient and sustainable future for the transportation sector.

Ethanol, derived from renewable sources like sugar cane and biomass, plays a vital role in the quest to reduce global reliance on non-renewable resources in the road transport sector. Its higher octane number compared to gasoline makes ethanol-gasoline blends essential for contemporary high compression ratio engines, leading to heightened engine efficiency. Additionally, when added to unleaded fuel, ethanol enhances knocking resistance, improves combustion performance, and reduces emissions of hydrocarbons (HC) and carbon monoxide (CO) in exhaust emissions. The characteristics of ethanol, such as an elevated heat of vaporization and reduced Reid Vapor Pressure, contribute to enhanced engine performance, lower emissions of volatile organic compounds during pumping, and a decrease in combustion temperatures, thereby reducing nitrogen oxides formation. Utilization of ethanol-gasoline blends holds promise in addressing environmental concerns, improving engine efficiency, and fostering sustainability in the face of environmental and health challenges associated with fossil-based fuels [10], [11].

1.2. Fuel Injection Systems

A key part of the fuel delivery system in internal combustion engines is the fuel injector. These components are intricately designed to atomize and deliver fuel in a finely dispersed mist to ensure efficient combustion. Fuel injectors consist of several intricate components, including the injector body, nozzle, pintle, solenoid, and sealing mechanisms such as O-rings. The injector body houses these components and is assembled within the engine, either mounted on the intake manifold or directly inside the combustion chamber. The nozzle, often designed with minute openings, ensures precise fuel spray characteristics, while the pintle and solenoid control the opening and closing of the nozzle to regulate fuel flow.

Two primary types of fuel injection systems are used in passenger vehicles: port fuel injection and gasoline direct injection (see Figure 1.2 [12]). The primary difference between the PFI engine and the GDI engine lies in their approaches to mixture preparation, which will be elaborated upon in Sections 1.2.1 and 1.2.2.

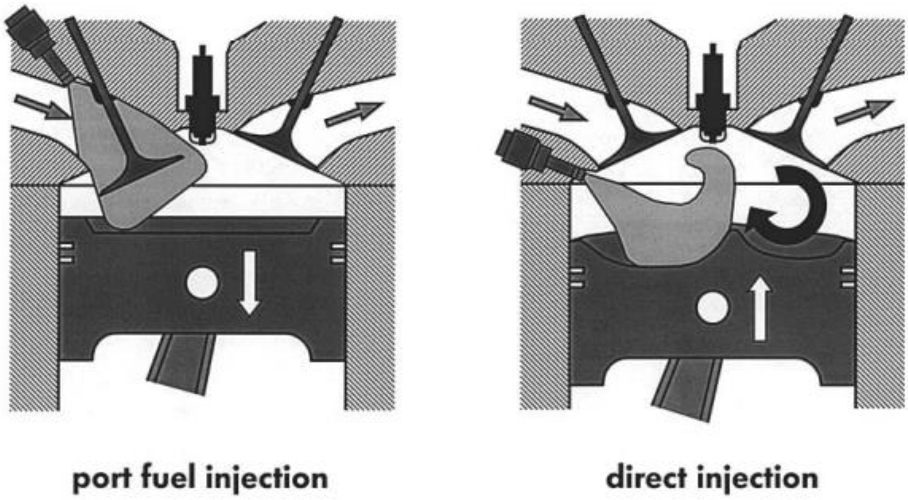

Figure 1.2 Gasoline Injection System

1.2.1. Port Fuel Injection (PFI)

Port fuel injection is a well-established and widely used system in the automotive industry. In PFI, the fuel injector is in the intake manifold, where it sprays a finely atomized mist of fuel just upstream of the intake valve (see Figure 1.3 [13]). As the intake valve opens and closes, it allows air to enter the combustion chamber while preventing air backflow. The fuel and air mixture is then ignited by the spark plug. PFI systems are known for their reliability, cost-effectiveness, and ability to provide a consistent air-fuel mixture. However, PFI may have limitations in terms of optimizing fuel-air mixing and achieving high compression ratios, which are essential for enhancing engine efficiency and reducing emissions.

Studies in the past had shown that enhancing the quantity of evaporated fuel within the injected fuel leads to improved fuel efficiency. The formation of a fuel film when the injected fuel interacts with the wall diminishes the amount of evaporated fuel in the combustion chamber, causing decreased fuel efficiency and serving as a significant factor in hydrocarbon (HC) emissions. In the case of port fuel injection (PFI) engines, some evaporated fuel inevitably lingers in the intake port. Nevertheless, by minimizing evaporated fuel in the intake port and maximizing it in the combustion chamber, fuel efficiency is enhanced, as combustion primarily occurs within the combustion chamber. The presence of liquid droplets, a result of non-evaporated injected fuel, further reduces the evaporated fuel mass in the combustion chamber, resulting in heightened NOx emissions and a decline in combustion stability [14].

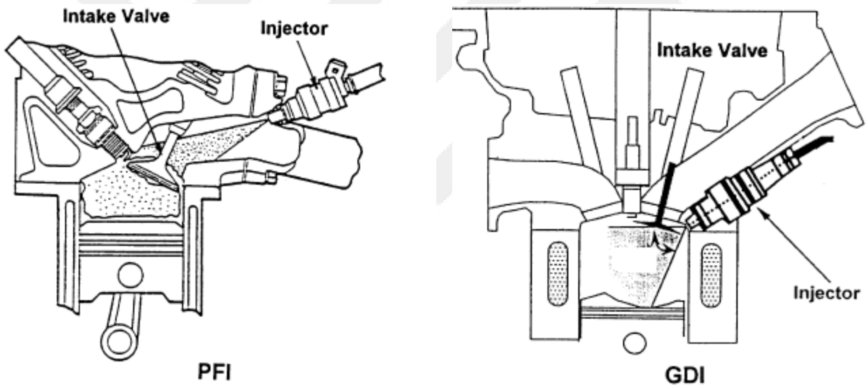

Figure 1.3 Comparison of the PFI and GDI Mixture Preparation Systems

1.2.2. Gasoline Direct Injection (GDI)

Gasoline direct injection is a more recent advancement in fuel injection technology. In GDI systems, fuel is directly injected into the combustion chamber at high pressure, typically through a multi-hole injector nozzle. This allows for precise control over the air-fuel mixture and injection timing, resulting in improved combustion efficiency, power output, and fuel economy. GDI systems are known for their ability to deliver fuel with remarkable precision, thereby reducing emissions and improving overall engine efficiency. However, they also present unique challenges related to fuel atomization, carbon buildup on the injector nozzles, and the need for exceptionally durable injector components to withstand the extreme conditions within the combustion chamber [15].

An article published in Environmental Science and Technology states that GDI vehicles emit roughly twice as much particulate matter (PM) mass as PFI vehicles, primarily due to higher elemental carbon emissions. Even though cold-start conditions significantly contribute to total unified cycle emissions, no significant differences in the effects of cold-start were observed between GDI and PFI vehicles. The research notes a 14.5% decrease in CO_2 emissions from GDI vehicles, which surpasses the potential climate impact associated with higher black carbon emissions. Therefore, transitioning from PFI to GDI vehicles is likely to result in a net reduction in global warming [16].

1.3. The Importance of O-Rings in Fuel Injectors

O-rings play a critical role in the functionality of both PFI and GDI fuel injectors. These small, circular sealing elements are typically made of elastomeric materials, such as rubber or silicone, and are strategically placed at various locations within the injector. O-rings are essential for creating a tight, leak-proof seal between different components and interfaces of the injector, ensuring that fuel is delivered accurately and efficiently. Furthermore, they help maintain the integrity of the fuel injector, preventing any leakage that may lead to engine malfunction, fuel waste, and, in some cases, safety hazards.

Though O-rings' main role is to prevent the leakage of fuel in the hydraulic connection, these components also interact with oils. Among the materials used for these seals, rubber stands out as the preferred choice due to its ability to maintain appropriate modulus against sealing surfaces, leveraging its viscoelastic characteristics. In this context, the choice of sealing materials, such as NBR, ACM, VMQ, and FKM, becomes pivotal, especially considering the demands for longer-lasting engine oils with lower viscosity to enhance fuel economy and performance at elevated temperatures.

As automotive engine oils are subjected to increasingly stringent requirements, including longer intervals between oil changes and improved lubrication efficiency, the development of synthetic lubricants has gained traction. However, the adoption of synthetic lubricants remains limited due to their higher cost and potential damage to rubber components. Consequently, the composition of engine oils, typically consisting of basic oil blended with additives, necessitates careful consideration to ensure compatibility with sealing materials, as certain additives may have adverse effects on elastomers commonly used in seals.

Hashimoto and his colleagues delve into the impact of various oil additives on elastomers, revealing that while some additives have minimal effects, others can significantly deteriorate the physical properties of elastomers like NBR. In contrast, ACM demonstrates stability against most additives, except for specific compounds. FKM, renowned for its resistance to heat and oil, is susceptible to certain additives, highlighting the complex interplay between additive formulations and elastomer properties. HNBR emerges as a promising option, boasting superior tensile strength and resistance to most oil additives [17].

Moreover, the discussion extends to the curing processes of FKM and the development of peroxide-cured variants to mitigate adverse reactions with certain additives. Additionally, the transition in engine gasket materials from NBR and cork rubber to ACM and VMQ underscores the importance of selecting materials that satisfy heat resistance and compression set requirements. Despite VMQ's superior flexibility and heat resistance under normal conditions, its susceptibility to degradation after prolonged exposure to engine oil contrasts with the resilience of FKM and ACM, highlighting the nuanced considerations in seal material selection for automotive applications.

1.3.1. Material Properties and Molecular Geometries of FKM

FKM, essential in various industries due to their outstanding resistance to heat, chemicals, and oils, are produced through a meticulous process involving the polymerization of specific monomers. Key monomers in this process include Vinylidene Fluoride (VF2), Hexafluoropropylene (HFP), and Tetrafluoroethylene (TFE). VF2, featuring a carbon-fluorine double bond, undergoes addition polymerization, wherein multiple VF2 monomers bond together to form polymer chains. Similarly, HFP and TFE, also fluorinated monomers, participate in the polymerization process through addition reactions, contributing to the formation of additional polymer chains.

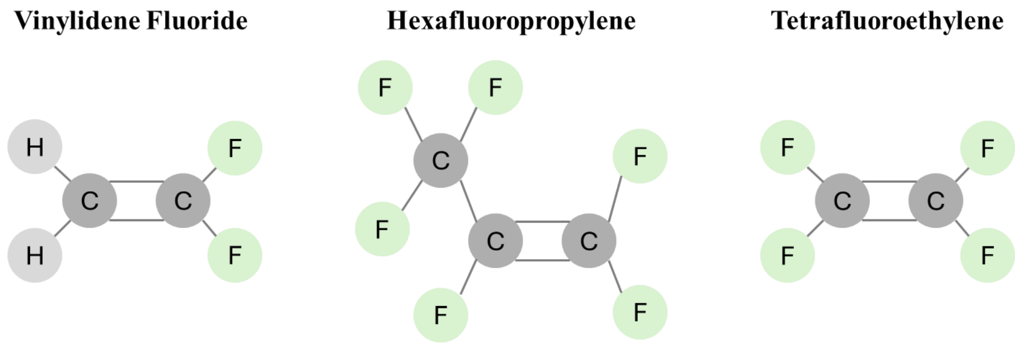

Figure 1.4 Monomers That Synthesis FKM

These monomers, along with various additives and processing agents, undergo polymerization through methods such as free-radical or emulsion polymerization. Additionally, cross-linking agents may be introduced to enhance mechanical properties. The resultant FKM material boasts a robust three-dimensional network structure characterized by strong carbon-fluorine bonds, enabling it to withstand harsh environmental conditions. This synthesis process plays a pivotal role in FKM production, facilitating their extensive utilization across industries where reliability and endurance are crucial.

FKM, evolving since the 1940s, has undergone significant chemical structural changes. Typically containing 66%-68% fluorine, FKM exhibits exceptional resistance to a wide range of aggressive substances, including acids, fuels, crude oil, and ammonia. The curing process has shifted from amine to bisphenol and peroxide. This high fluorine content, coupled with the utilization of various monomers like VF2, HFP, TFE, PAVE/PFVE, Ethylene, and Propylene in its production, imparts distinct properties to FKM, ranging from performance in ultra-low temperatures to heightened resistance against acids and bases [18].

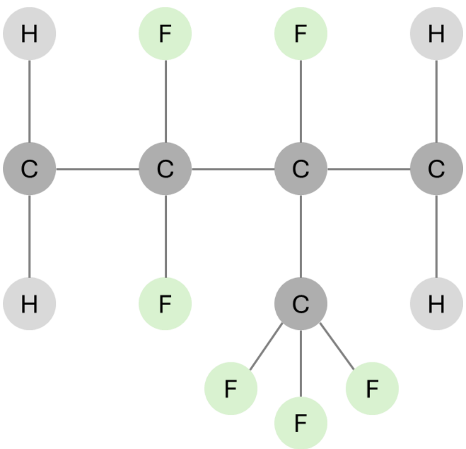

Figure 1.5 Molecular Structure of FKM

FKM, like the well-known Viton™, have gained considerable recognition across different industries for their outstanding qualities and performance. Praised for their remarkable resistance to chemicals, stability under heat, and durability, these synthetic rubbers are highly valued in demanding settings [19]. Their ability to endure corrosive substances such as acids, bases, oils, and solvents while maintaining their integrity across a broad temperature range from -20 °C to over 200 °C highlights their adaptability and reliability. Moreover, FKM's resilience under prolonged mechanical stress without compromising its sealing effectiveness, alongside its natural flexibility, elasticity, and resistance to wear, ensures consistent performance in crucial applications such as automotive, aerospace, and chemical processing [20]. As ongoing advancements in formulation and processing techniques continue to shape FKM's development, its pivotal role as a foundational material in modern engineering becomes increasingly apparent, meeting the rigorous demands for performance, reliability, and durability in various fields. Whether it's sealing automotive engines, hydraulic systems, aerospace components, or industrial machinery, FKM remains at the forefront, embodying a blend of innovation, reliability, and excellence that characterizes cutting-edge engineering materials.

1.4. O-Ring Vulnerability to Fuel Type

The compatibility of O-rings with various fuel types is a crucial concern when adapting fuel injectors to alternative fuels like ethanol. Ethanol, unlike conventional gasoline, possesses distinct chemical and physical properties that can have a direct impact on O-ring performance and longevity. Among the critical material properties that affect O-ring performance when exposed to different fuel types are hardness, tensile strength, and elongation.

While extensive research has been conducted on the physical property changes of elastomers when exposed to biodiesel blends, there is a notable gap in the literature regarding similar investigations with gasoline-ethanol blends. Biodiesel's impact on elastomers has been extensively studied due to its increasing use as a substitute for fossil diesel in compression ignition engines. Previous research has focused on parameters such as combustion characteristics and environmental impact, highlighting both the benefits and challenges associated with biodiesel utilization. For instance, biodiesel's oxidative properties have been found to enhance corrosion and material degradation, particularly affecting elastomers and metallic components in diesel vehicle fuel systems. However, while biodiesel studies provide valuable insights into material compatibility and durability, there is limited literature available to reference the effects of gasoline-ethanol blends on elastomers in automotive applications.

As outlined in the study, which investigated the changes in physical properties of various elastomers exposed to rapeseed oil biodiesel, the research revealed significant impacts on elastomers such as FKM (fluorocarbon material), among others. While B100 exhibited a more pronounced effect compared to petroleum diesel (B0), both fuels caused changes in elastomers, albeit to varying degrees. Notably, FKM demonstrated higher compatibility with biodiesel blends, maintaining similar properties even after immersion. However, this study underscores the need for further research to understand the degradation mechanisms and develop more durable FKM elastomers for use in automotive fuel systems. Therefore, in the absence of comprehensive literature on the effects of gasoline-ethanol blends on FKM elastomers, this biodiesel study serves as a valuable reference point for understanding material compatibility and guiding future research endeavors in alternative fuel applications [21].

1.4.1. Hardness

O-ring hardness is a measure of the material's resistance to deformation when subjected to compressive forces. The hardness of an O-ring material is typically measured on standardized scales such as the Shore A or Shore D durometer scales. When exposed to ethanol-based fuels, O-rings with inadequate hardness may experience excessive compression, leading to a loss of sealing integrity. Conversely, O-rings that are too hard may become brittle, making them susceptible to cracking and failure when subjected to dynamic loads. Therefore, finding the optimal hardness for O-ring materials is essential to ensure proper sealing performance and long-term durability in fuel injectors utilizing ethanol-based fuels.

According to study conducted by Kass and his colleagues, it was found out that the decrease in hardness level has a correlation with increase in volume of specimen. Experiments on FKM specimens had shown that volume expansion under media is roughly twice the mass increase (wet state); meanwhile, the wet hardness decreases by average of 10 Shore-A points. However, when specimens were dried followed by immersion, the results had dropped significantly compared to wet state results. In short, study proves that specimens get softer when subjected to abrasive fuels such as ethanol blends [22].

1.4.2. Tensile Strength

Tensile strength is the maximum amount of tensile (pulling) stress that a material can withstand without breaking. When O-rings are exposed to ethanol-based fuels, tensile strength becomes critical because these fuels may alter the material's structural integrity over time. O-ring materials with lower tensile strength may become more susceptible to elongation, deformation, and ultimately, failure under stress. On the other hand, materials with high tensile strength are better equipped to withstand mechanical and hydraulic forces and maintain their sealing properties. Investigating the effect of ethanol-based fuels on O-ring tensile strength is a fundamental aspect of understanding their performance in fuel injector applications.

Due to pressure cycles in the powertrain system, the swollen shape of O-ring differs at each hydraulic pressure unit. During these cycles, O-ring gets compressed or decompressed. With enough applied pressure on O-rings, internal crack formations start to occur. Once this happens, the crack formation will get bigger with decompression action. This mechanism is explained by the tear energy built up in compressed state of O-ring, and the release of this energy at during or after decompression state. Therefore, the chosen O-ring for application must withstand the combined pressures of compression and hydraulic press [23].

1.4.3. Elongation

Elongation measures the ability of a material to stretch or deform before breaking. When O-rings are exposed to ethanol-based fuels, elongation is a key consideration because the material may experience mechanical stress, such as stretching or compression during operation. O-ring materials with inadequate elongation characteristics may lose their ability to maintain a secure seal when subjected to dynamic conditions within the injector. In contrast, materials with greater elongation properties can better accommodate the mechanical stresses and maintain their sealing efficiency. Evaluating the impact of ethanol-based fuels on O-ring elongation is essential for assessing their overall performance in real-world applications.

1.5. Hydraulic Interface and Importance of its Optimization

Within the intricate realm of fuel injection systems, the hydraulic link between the fuel rail and the injector plays a pivotal role, significantly affecting injector performance. The fuel rail, serving as a high-pressure conduit, functions as the central hub for distributing pressurized fuel to individual injectors, ensuring the consistent delivery of fuel precisely when needed.

Optimizing this hydraulic interface between the fuel rail and injector is paramount to ensure the fuel injector operates at its maximum efficiency. Any irregularities or interruptions in this interface can result in uneven fuel distribution among cylinders, leading to suboptimal combustion, reduced engine efficiency, and increased emissions. In this context, the role of O-rings and other sealing components within the hydraulic connection becomes particularly critical.

Li conducted a thorough investigation into the behavior of O-ring seals in high-pressure environments, utilizing finite element analysis (FEA) as the primary analytical tool. The study focused on exploring the impacts of varying compression rates, static pressures, and motion speeds on the equivalent stress and contact stress experienced by the O-ring seals. Through the development of finite element models and simulations that replicated diverse operational scenarios ranging from installation processes to hydrostatic loading and reciprocating motion, Li systematically examined the performance of O-ring seals under different conditions. The research revealed that increasing the compression rate during installation enhances the sealing effectiveness of O-rings, albeit with potential drawbacks such as stress concentration and residual deformation. Furthermore, the findings elucidated complex relationships between static pressure, motion speed, and stress distribution during reciprocating motion, underscoring the multifaceted nature of these interactions. Such insights hold significant implications for the optimization of hydraulic connections, offering valuable guidance for enhancing system efficiency and durability by addressing stress-related challenges in O-ring seals [24].

The compatibility of O-rings with ethanol-based fuels and their ability to establish a dependable seal at the hydraulic interface are fundamental in achieving uniform fuel delivery. If O-rings fail to maintain a secure seal, it can lead to fuel leaks or pressure losses, compromising the overall engine performance and efficiency. The importance of optimizing O-rings at this critical junction cannot be overstated.

This thesis embarks on a comprehensive exploration of the hydraulic connection between the fuel rail and injector, shedding light on how ethanol-based fuels impact O-ring performance and sealing properties within this specific context. Through a systematic analysis, the objective is to gain a deeper understanding of how O-rings interact with ethanol at the hydraulic interface and how optimization strategies can be applied to ensure a consistent and reliable seal. The ultimate goal is to contribute to the development of fuel injection systems that not only accommodate alternative fuels like ethanol but also excel in meeting the efficiency requirements of modern passenger vehicles.

2. MATERIAL AND METHODS

This chapter covers how the test specimen was chosen, which medias were used and how the tests were carried out; moreover, determination of input parameters for simulation is explained with the simulation conditions.

The process of selecting an appropriate test specimen holds significant importance when exploring material characteristics, particularly in the context of crucial components like O-rings utilized. In this study, the chosen test specimen comprises an O-ring made of FKM (fluorocarbon-based fluoroelastomer) with dimensions of 4.45 x 3 (ID x (OD-2 ID)) which is also the O-ring used in HDEV6 injectors (see Figure 2.1).

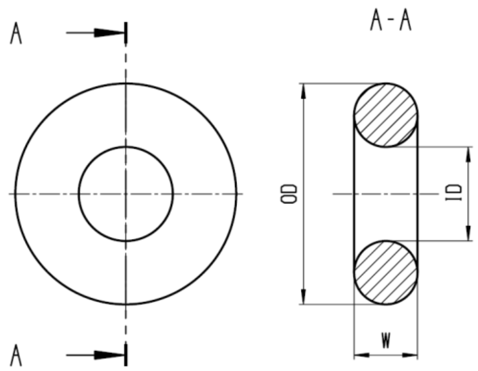

Figure 2.1 O-ring Dimensions and Its Cross-Section View

The reasons behind why this O-ring dimensions were selected are stated below.

2.1.1. Real-world Applications

For meaningful research, it is imperative that the test specimen closely reflects real-world applications. By opting for an O-ring with identical dimensions to those found in HDEV6 injectors (4.45 x 3), the objective is to assess the material properties and performance attributes of O-rings under conditions directly relevant to the system in question.

2.1.2. Standardization and Comparability

Standardization is a fundamental aspect in scientific investigations that facilitates result comparison and reproducibility. Using a known dimension O-ring ensures that test conditions can be consistently duplicated and compared with future studies or industry benchmarks. This enhances the reliability of research findings.

2.1.3. Material Properties Focus

O-rings are typically made from various materials, and in this case, it is made of FKM. The material is known for its exceptional performance in extreme conditions. This specific material exhibits remarkable properties, such as outstanding elasticity, durability, and resistance to temperature and pressure. FKM can operate effectively within a wide temperature range, from -40 °C to 150 °C at 350bar. This property ensured that the material would not deteriorate at extreme conditions.

2.1.4. Accessibility and Availability Considerations

Another practical aspect is the ease of obtaining O-rings with the specified dimensions. These components are readily accessible, making the study cost-effective and logistically feasible within the constraints of the research timeline.

2.2. Media Used in Testing and Immersion Test Followed by Drying

In this research, the assessment of O-ring behavior involved the utilization of various gasoline blends, including E10, E30, E85, and E100, as these are the maximum ethanol-containing gasoline blends regulated by various countries worldwide (Figure 2.2 [25]). Additionally, an immersion test was conducted in which O-rings were placed within sealed 100ml bottles for a duration of 168 hours with the purpose of allowing a direct comparison between the dry-state and immersed-states of the O-rings, which was essential for evaluating the effect of the test media.

Figure 2.2 Worldwide Used Gasoline Blends

Below is a detailed explanation of these test media and procedures:

2.2.1. Gasoline Types

The choice of E10, E30, E85, and E100 as the test media was driven by their relevance to real-world applications. These specific gasoline blends were selected due to their prevalence in various international markets and their varying ethanol content, which can have a significant impact on material compatibility. E10 represents a blend of 10% ethanol with gasoline, while E30, E85, and E100 consist of higher ethanol proportions at 30%, 85%, and 100%, respectively (Table 2.1). These ethanol-gasoline blends are subject to regulatory standards in different regions, and the evaluation of O-ring performance under such conditions is crucial for understanding their behavior in practical applications.

Table 2.1 Gasoline-Ethanol Blends for Testing

Gasoline Blend	Ethanol Content [%]	Gasoline Content [%]
E10	10	90
E30	30	70
E85	85	15
E100	100	0

2.2.2. Procedure of Immersion Test and Drying

The immersion test was conducted in accordance with the ISO 1817 standard to ensure consistency and conformity with established testing protocols [26]. For each gasoline variant (E10, E30, E85, E100), a total of 5 O-rings were individually placed within separate 100ml bottles, following ISO 1817 guidelines, which provide a recognized framework for assessing the resistance of rubber materials to liquid chemicals. The bottles were securely sealed to create a controlled environment for each specimen.

After completion of the immersion tests, it was imperative to prepare the O-rings by ensuring they were completely dry to eliminate any potential moisture interference during the test. To achieve this, the O-ring samples were subjected to a thorough drying process. They were placed within a specialized TW-S machine and exposed to a temperature of 80 °C for a duration of 12 hours. This controlled drying procedure ensured that the O-rings were in an optimal, moisture-free state before being immersed in the test media. Proper preparation of the O-rings in accordance with ISO 1817 guidelines, including the drying process, was crucial to the accuracy and reliability of the subsequent immersion tests, allowing for an accurate assessment of O-ring behavior when exposed to the designated gasoline types.

2.2.3. Phase Separation Behavior in Gasoline-Ethanol Blends

In gasoline-ethanol blends, the potential for phase separation is a well-known occurrence affected by environmental conditions and time. This phenomenon arises due to the different solubility properties of ethanol and gasoline. Ethanol has a higher affinity for water, so even a small amount of moisture can trigger phase separation as ethanol tends to form a separate phase with water. Moreover, changes in temperature, pressure, and humidity can worsen phase separation by altering the equilibrium between the blended components.

The process of separation involves the formation of distinct ethanol-rich and gasoline-rich phases. Over time, gravity causes the denser ethanol-rich phase to settle at the bottom while the lighter gasoline-rich phase remains on top. Environmental factors like temperature variations and agitation can speed up this separation process.

However, it's important to note that phase separation isn't always inevitable. In controlled laboratory settings, like the one used in this study with sealed flasks, steps were taken to minimize external influences and maintain consistent conditions. Density measurements taken at different levels and time points showed no signs of phase separation. This suggests that the experimental setup effectively prevented conditions that could lead to separation, highlighting the importance of controlled environments when studying gasoline-ethanol blends.

2.2.4. Test Equipment for Immersion Tests:

The immersion tests were conducted in accordance with Method-B outlined in ISO 1817 to evaluate the resistance of O-ring specimens to various gasoline-ethanol blends. For each test, 100 mL glass bottles were utilized, each filled with 50 mL of the respective gasoline-ethanol blend. Subsequently, O-ring specimens were placed into the filled bottles, and the lids were securely closed to ensure a sealed environment during the immersion period.

To facilitate comprehensive testing across different gasoline-ethanol blends, a total of 20 glass bottles were employed, distributed as follows: 5 bottles containing E10 blend, 5 bottles containing E30 blend, 5 bottles containing E85 blend, and the remaining 5 bottles containing E100 gasoline-ethanol blend. This selection of blends represents a range of ethanol concentrations commonly encountered in automotive fuel formulations, allowing for a thorough investigation of the O-ring's resistance under varying environmental conditions.

Following the placement of O-ring specimens into the respective bottles, the sealed flasks were stored for a duration of 168 hours to simulate prolonged exposure to the gasoline-ethanol blends. This extended immersion period enables the assessment of the O-ring's durability and performance under realistic operating conditions, including potential long-term effects of exposure to the test fluids.

To provide visual context and enhance the understanding of the experimental setup, Figure 2.3 below depicts the glass bottle used for the immersion tests, illustrating the sealed environment created for evaluating the O-ring specimens' resistance to the gasoline-ethanol blends.

By utilizing the described test equipment and methodology, we aimed to comprehensively evaluate the compatibility and resistance of O-ring specimens to various gasoline-ethanol blends, thereby informing engineering considerations for applications in automotive fuel systems and related industries.

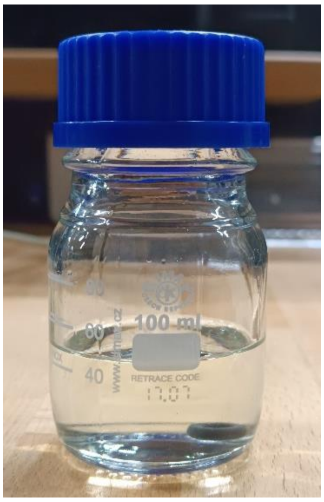

Figure 2.3 Glass Bottle Setup for Immersion Tests

2.2.5. Machine for Drying O-rings

After subjecting the O-ring specimens to immersion tests with various gasoline-ethanol blends per ISO 1817 Method-B, a drying process was conducted to eliminate residual moisture and restore the O-rings' original characteristics. The Vötsch VT3 7012 S2 drying machine was utilized for this purpose, providing controlled drying conditions to effectively remove moisture from the specimens.

The Vötsch VT3 7012 S2 drying machine offers precise temperature regulation and uniform heat distribution, ensuring consistent and dependable drying outcomes. O-ring specimens were positioned within the drying chamber and exposed to a stable temperature of 80 °C for a duration of 12 hours. This extended drying period facilitated thorough moisture evaporation, preventing potential material degradation and ensuring the O-rings' suitability for subsequent testing and analysis.

A visual depiction of the Vötsch VT3 7012 S2 drying machine setup is presented in Figure 2.4 below. Additionally, Table 2.2 outlines the essential specifications of the drying machine, such as temperature range and heating capacity, providing further insight into its role in the experimental process [27].

Figure 2.4 Vötsch VT3 7012 S2 Drying Machine

Table 2.2 Specifications of Vötsch VT3 7012 S2 Drying Machine

Type	VT^3 7012 S2
Test space volume	60 Litre
Amount of Zones	2
Temperature range hot zone	+50 to +220 °C
Temperature range cold zone	-80 to +70 °C
Temperature deviation in time	±0.3 to ±1.0 K
Temperature homogenity in space relative to set value	±0.5 to ±2.0 K
Calibrated values	
Cold zone	-40 °C
Hot zone	+125 °C
Test space dimensions	
Width	470 mm
Depth	650 mm
Height	410 mm
External dimensions	
Width	970 mm
Depth	2350 mm
Height	1985 mm
(…)[3]	2450 mm
Loading capacity max	50 mm
Sound pressure level	56 mm
Refrigeration unit	water-cooled
Control System	SIMPAC
Electrical connection	3/N/PE AC 400V ± 10%, 50Hz
Rated power	10 kW

By employing the Vötsch VT3 7012 S2 drying machine, effective moisture removal from the O-ring specimens post-immersion was achieved, safeguarding the reliability and integrity of the test results.

2.3. Hardness Test

The hardness assessment stands as a crucial element within this research, with the primary objective of appraising the mechanical attributes of O-rings. In the realm of elastomeric materials such as O-rings, hardness pertains to their capacity to resist deformation or impressions. This examination functions as a gauge of the O-rings' capacity to endure compressive forces and is of paramount importance in gauging their appropriateness for distinct applications.

2.3.1. Determination of Hardness Method

Even though there are various hardness measurements methods (e.g. Shore-A, Shore-D, etc.), IRHD methods was preferred for testing. Compared to other hardness measuring methods, IRHD has brings its own advantages.

During hardness measurements, an indenter gets pressed onto the surface of specimen for a specific time with a controlled force. In Shore-A and Shore-D methods, the indenters have sharp edges (see Figure 2.5 for indenter shapes [28]). Once these tools are pressed on, they leave a surface defection on the specimen which makes them unusable for application. However, in IRHD method, the indenter has spherical shape. When such geometry is used, it leaves much less deformation compared to Shore methods.

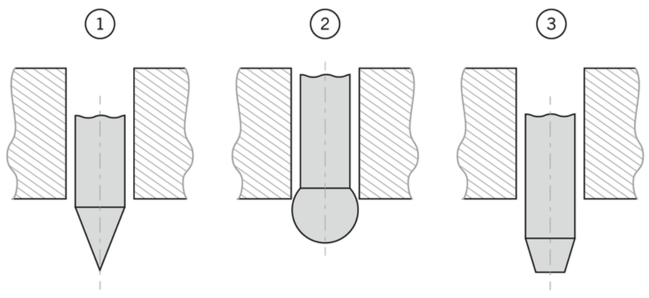

Figure 2.5 Types of Hardness Indenters 1) Conical 2) Spherical 3) Truncated Cone

Additionally, the precision of Shore-A hardness assessments can be influenced by variables such as the rate of force application and the duration of force application. When dealing with highly pliable materials, it becomes even more imperative to meticulously manage these factors to ensure the acquisition of accurate results. Since IRHD provides higher accuracy and precision, it is a more preferable method in elastomer hardness measurements.

2.3.2. IRHD Measurement Device

The IRHD Compact III machine, manufactured by Bareiss, was employed to conduct IRHD method M hardness tests on O-ring specimens in accordance with ISO 48 standard [29]. This particular machine was chosen for its capability to precisely measure the indentation hardness of rubber materials while minimizing damage to the O-ring samples. The IRHD Compact III is well-regarded for its accuracy in assessing the hardness of rubber materials, making it an ideal choice for evaluating O-ring hardness without significantly altering their properties. Its advanced technology ensures consistent and dependable results, enhancing the reliability and reproducibility of hardness measurements during testing.

A detailed summary of the machine's properties is presented in Table 2.3, which includes key specifications such as testing range and resolution. Furthermore, visual representation of the machine's setup is provided in Figure 2.6 to aid in understanding its configuration [30].

Figure 2.6 Bareiss IRHD Compact III Machine

Table 2.3 IRHD Compact III Technical Properties

Voltage	Power supply setINPUT: 100 – 240 VAC; 50/60 HzOUTPUT: 3,3 VDC
Protection class	IP 50
Resolution	0.1 IRHD
Measuring range	IRHD M / IRHD N
Measuring time	1 - 99 s

Data output	V24 RS 232 - 9600 Baud, 1 Start bit, 8 Data bits, 1 Stop bit
IRHD M	
Total Force	153.3 mN
Force on foot	235 mN
Indenterball Ø	0.4 mm
Measuring distance	0.3 mm
Range of reading	30-100 IRHD

Through the use of the IRHD Compact III machine, precise measurements of O-ring indentation hardness were obtained, facilitating a thorough assessment of their mechanical properties.

2.3.3. Steps of IRHD Testing

Tests performed in this section were according to the ISO 48-3 and ISO 48-4. O-ring hardness tests were performed at (23 ± 2) °C and below procedures were carried out to get values stated in (2.1); where F represents the applied force (in Newtons) during testing, R represents recovery force (in Newtons) after removing the indenter, and D represents depth of indentation (in millimeters).

$$IRHD = (F - R)/D \tag{2.1}$$

Flow steps of testing:

1. Placing O-ring on testing plate.
2. Calibrating the IRHD testing machine.
3. Applying force to the spherical-tipped plunger, pressing it into the surface of the O-ring.
4. Recording the force applied (F) and the depth of indentation (D).
5. Removing the plunger and allowing the material to recover to a certain extent. Recording the recovery force (R) after the plunger has been removed.
6. Pluging the recorded values (F, R, and D) into the formula, and calculating the IRHD hardness value.

2.4. Tensile Strength Test

The evaluation of the O-ring's intrinsic strength through the Tensile Strength Test holds a critical role in quality control. O-rings, serving as hydraulic system seals, undergo tensile stresses during assembly. Their capability to endure stretching and prevent premature failure is of utmost importance for upholding seal reliability, preventing leaks, and preserving system integrity. Thus, stress and strain behavior must be validated before application.

Considering the O-ring's deployment in high-stakes environments where failure can lead to severe consequences, it becomes imperative to ensure that its tensile strength remains within specified limits, effectively averting the potential for catastrophic failure that could result in system malfunctions or environmental hazards.

2.4.1. Tensile Strength Machine and Fixture

The tensile strength tests conducted on O-ring specimens were performed utilizing the Zwick Roell Zwickline Z2.5 materials testing machine. This specific machine was chosen due to its capability to precisely measure the tensile properties of materials by subjecting specimens to controlled forces until failure occurs. The machine is renowned for its accuracy, reliability, and versatility in materials testing applications. It offers a comprehensive analysis of the mechanical behavior of materials through the recording of force versus displacement data, which is then graphically represented using dedicated software provided with the machine.

Table 2.4 Properties of Zwick Roell Zwickline Z2.5

Type	Z2.5 TS
Item No.	59001
Test load Fmax	2.5 kN
Test area	
Moving crosshead mounted with angle up	235 - 565 mm
Moving crosshead mounted with angle down	90 - 420 mm
Depth	105 mm
Load frame	
Height without top crosshead	789 mm
Width	408 mm
Width with machine electronics	411 mm
Depth	480 mm
Depth with machine electronics	622 mm
With machine electronics, approx.	68 kg
Average noise level at v_{max} measured at 1 m distance from the front of the machine	55 dB(A)
Drive System	
Crosshead speed v_{min} - v_{max}	0.0005 - 1000 m/min
Drive travel resolution	0.0277 µm

A detailed overview of the properties of the Zwick Roell Zwickline Z2.5 machine is presented in Table 2.4 above [31]. This table includes essential specifications such as its maximum load capacity, displacement resolution, testing speed range, and any other pertinent technical details necessary for understanding its performance in the context of the tensile strength tests conducted on O-ring specimens. Additionally, visual representations of the Zwick Roell Z2.5 machine, including its configuration and setup, are provided in Figure 2.7 enhanced clarity and reference.

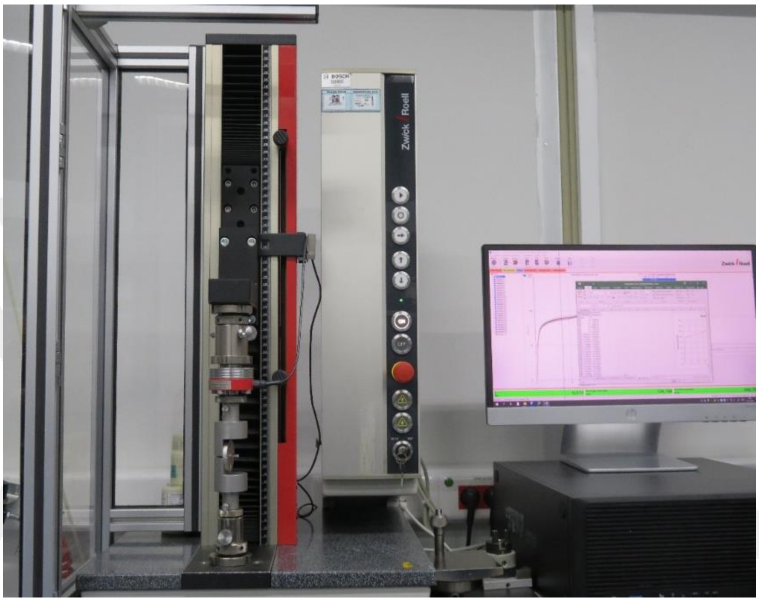

Figure 2.7 Zwick Roell Zwickline Z2.5 and Software

By utilizing the Zwick Roell Zwickline Z2.5 materials testing machine, precise and reliable measurements of the tensile properties of O-ring specimens were ensured, thereby contributing to the accurate characterization of their mechanical behavior under tensile loading conditions.

In conjunction with the machine, a custom fixture was assembled to facilitate the tensile strength tests on O-ring specimens. This fixture was specifically designed to securely hold the O-ring specimens in place during testing, ensuring consistent and reliable results. The fixture allows for easy insertion of the O-ring onto its designated position, providing a stable configuration for testing purposes.

During the testing procedure, as the machine applies controlled forces to the specimen, the custom fixture ensures that the O-ring remains securely positioned and aligned, minimizing any potential slippage or misalignment that could affect the accuracy of the test results. The fixture is engineered to withstand the forces exerted during testing while maintaining the integrity of the O-ring specimen under evaluation.

An illustration of the custom fixture assembly, including its configuration and integration with the Zwick Roell Z2.5 machine, is provided in Figure 2.8 below. This visual representation offers insight into the setup used for conducting the tensile strength tests on O-ring specimens, enhancing the understanding of the experimental procedure and equipment utilized in the study.

a)

b)

Figure 2.8 a) O-ring Mount Fixture, b) O-ring Mounted on the Fixture

By incorporating the custom fixture assembly into the experimental setup, we ensured precise positioning and consistent testing conditions for evaluating the tensile properties of O-ring specimens, thereby enhancing the reliability and accuracy of the experimental results.

2.4.2. Tensile Strength Test Procedure

The test was performed according to below steps:

1. Two semicircular discs with radius of 2.5mm were mounted on the ZwickLine machine in such a way that they could act as fixtures. Discs were aligned for coaxiality and they were brought to each other until they slightly touched and formed a full-disc (see Figure 2.9).

2. O-ring was placed on top of these discs, ensuring that it was evenly aligned along the axis of testing.
3. Configured the ZwickLine machine to record force versus displacement during the test with the following inputs:
   a. v=5 mm/min at $F_{min} \leq 0.5$ N
   b. v=200 mm/min at $F_{min} \geq 0.5$ N
   4. Initiated the test by starting the ZwickLine machine.
   5. The two discs had moved apart, causing the O-ring to stretch along its axis.
   6. Continuously recorded the force applied to the O-ring and the corresponding displacement as it stretched.
   7. Test had continued until the O-ring reached its breaking point, at which it ruptured; and the machine automatically stopped the test upon O-ring failure.
   8. Recorded data was converted to excel file and post-processed for stress and strain values with Equation (2.2) - (2.4).

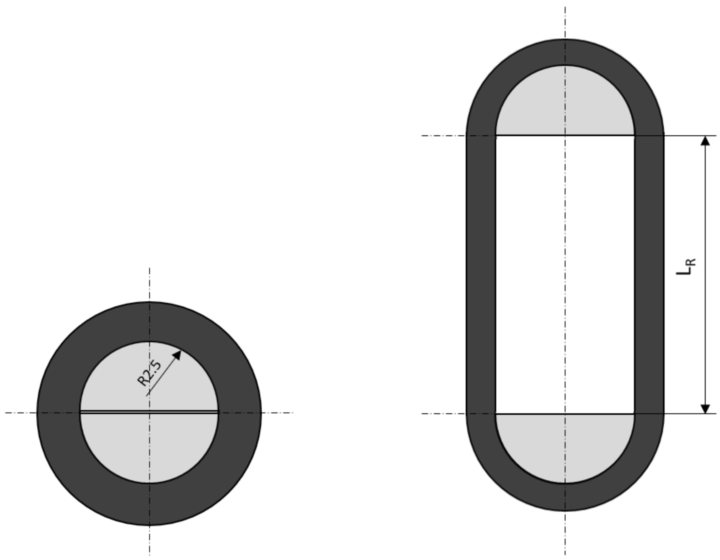

Figure 2.9 O-ring Tensile Strength Test Setup; Initial Step Is Shown at Left Hand Side, Whereas Final Step Is Shown On Right

Upon completion of test, strain and stress values were calculated analytically with the Equation (2.3) and (2.4).

$$A_0 = \frac{\pi}{4} \times W^2 \qquad (2.2)$$

$$\varepsilon_R = (L_R - L_0)/L_0 \times 100 \quad (2.3)$$

$$\sigma_{max} = \frac{F_{max}}{2A_0} \quad (2.4)$$

2.5. Optimization of Hydraulic Connection

2.5.1. Parametric Study of FKM O-ring Dimensions and Piston Diameter

The optimization of the hydraulic connection in gasoline injectors involves a comprehensive parametric study focusing on the dimensions of the FKM O-ring and the diameter of the piston. The objective is to understand the influence of these parameters on critical sealing attributes, including overall squeeze, groove fill, and contact pressure. This study is particularly relevant for various types of seals employed in gasoline injectors, such as radial and axial sealing components, including rod seals, piston seals, and face seals.

2.5.1.1. Initial Sealing Configuration

To establish a baseline for the parametric study, an initial set of dimensions for the FKM O-ring and piston diameter is referenced from HDEV6. These starting conditions will serve as a reference point for subsequent investigations. The parametric study involves systematic variations in the dimensions, incrementing stepwise from the initial configuration.

2.5.1.2. Radial Piston Seal Design

The sealing mechanism employed in this study is the radial piston seal, a crucial component in gasoline injectors. The radial piston seal is designed to operate under pressure from one side, effectively preventing leakage in high-pressure environments. Its unique design ensures effective sealing between the piston and cylinder bore.

The radial piston seal functions by utilizing the radial force generated during the interaction between the piston and the sealing element. As pressure is applied, the seal is forced against the cylinder bore, creating a tight radial contact. This design is particularly suitable for applications where high pressure differentials are encountered, making it ideal for gasoline injector systems.

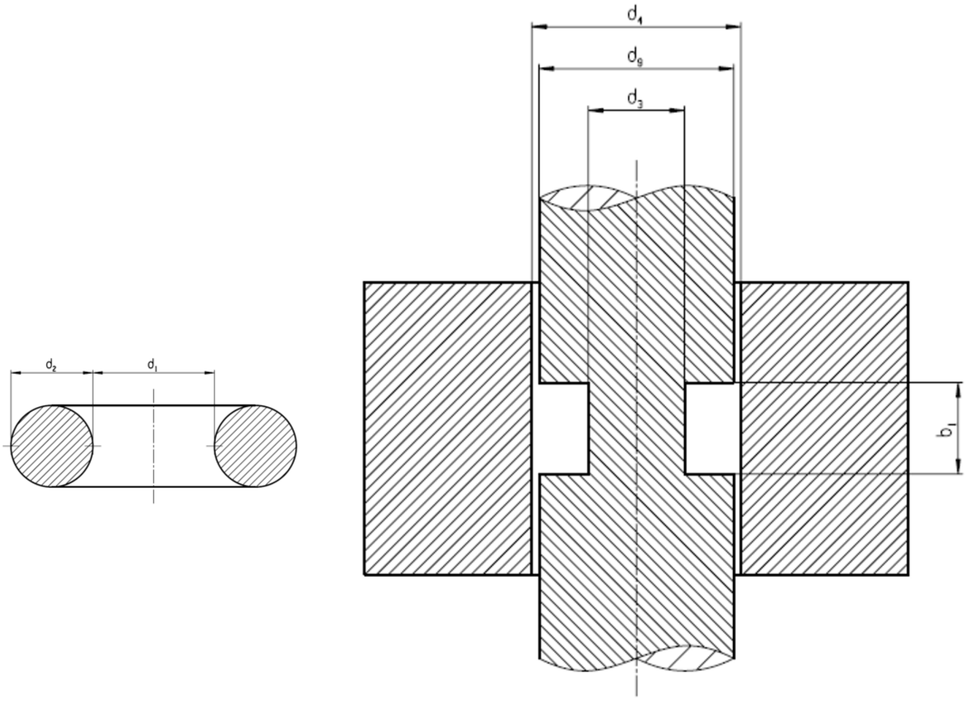

Figure 2.10 Radial Piston Seal Design

Table 2.5 Initial Dimension for Hydraulic Interface Optimization Study

Parameter	**Dimension [mm]**
d_1	4.45
d_2	3.00
d_3	4.60
d_4	9.40
d_9	9.32
b_1	4.37

2.5.1.3. Initial Stretch

The significance of the Initial Stretch of O-rings becomes evident in the realm of radial piston O-ring sealing. This term denotes the pre-deformation or pre-compression applied to an O-ring before it is placed in a sealing groove. In radial piston scenarios, where effective sealing is paramount, a thorough understanding, and calculation of the initial stretch prove pivotal for assorted reasons.

Ensuring proper adherence to the sealing groove geometry, the Initial Stretch plays a crucial role in establishing a secure and uniform seal. This adherence is essential for averting leakage and extrusion challenges, especially in high-pressure environments commonly encountered in radial piston systems. Moreover, the carefully determined Initial Stretch contributes to an augmented sealing force, bolstering the O-ring's resilience in dynamic operational conditions. Through the optimization of this parameter, engineers can enhance temperature and pressure stability, ultimately prolonging the lifespan of the O-ring seal and ensuring steadfast performance in radial piston applications.

$$S_{initial} = \frac{d3 - d1}{d1} * 100\% \quad (2.5)$$

2.5.1.4. Compression

The compression of the radial piston sealing is a key factor in ensuring effective sealing under pressure. The parametric study will investigate the variation in compression within the acceptable range of 10% to 30% based on the limits referred in standards and handbooks. ISO 3601-01 states that in order to calculate compression (C), cross section reduction due to diameter stretch (R) and effective cross section (d_2') must be found out [32] - [34].

$$R = 0.056 + 0.59(S_{initial}) - 0.0046(S_{initial})^2 \quad (2.6)$$

$$d_2' = d_2 - \frac{R}{100} * d_4 \quad (2.7)$$

With the found effecting cross section diameter, compression can be calculated according to below formula:

$$C = \frac{d_2' - t}{d_2'} * 100\% \quad (2.8)$$

where (t) is the distance between wall and groove diameter ($t = d_4 - d_3$).

2.5.1.5. Groove Fill

Understanding the groove fill is crucial for assessing the effectiveness of the sealing mechanism. The parametric study explores the groove fill (G_{fill}) and its sensitivity to temperature variations. The calculation for groove fill incorporates the thermal expansion effect:

$$G_{fill} = \frac{V_{O-ring}}{V_{groove}} * 100\% \tag{2.9}$$

where (V_{O-ring}) and (V_{groove}) are the volumes of the O-ring and the groove, respectively.

$$V_{O-ring} = (d_1 + d_2) * (d_2^2) \tag{2.10}$$

$$V_{groove} = \pi * \frac{d_4^2 - d_3^2}{4} * b_1 \tag{2.11}$$

2.5.1.6. Contact Pressure

Contact pressure is a critical parameter influencing the sealing performance. The study analyzes the change in contact pressure ($P_{contact}$) resulting from variations in O-ring dimensions and piston diameter. To calculate the pressure, force and contact width of O-rings must be calculated in advance. Lindley had proposed that Equation (2.13) and (2.14) can be used to find out these values [35], [36].

$$\delta = C \,/\, 100 \tag{2.12}$$

$$\frac{F_{axial}}{\pi d D E} = 1.25(\delta)^{3/2} + 50(\delta)^6 \tag{2.13}$$

$$\frac{\pi}{6}\left(\frac{a}{d}\right)^2 = 1.25\delta^{3/2} + 50\delta^6 \tag{2.14}$$

Where F, d, D, E, a represent contact force, cross section diameter (d_2), mean diameter ($d_1 + d_2$), modulus of elasticity and contact width respectively.

The contact pressure is computed using the following equations:

$$A_{contact,piston} = a\pi d_1 \tag{2.15}$$

$$A_{contact,bore} = a\pi(d_1 + 2d_2) \tag{2.16}$$

$$P_{contact} = \frac{F_{axial}}{A_{contact}} * 100\% \tag{2.17}$$

2.5.2. Influence of O-ring Hardness on Sealing Performance

Building on the results obtained from the parametric study, the next phase investigates the impact of O-ring hardness on either contact pressure or radial force. This analysis aims to establish trends and correlations between O-ring hardness and sealing attributes, providing valuable insights into the material properties' influence on hydraulic connection optimization. The relationship between O-ring hardness and sealing performance will be explored through a series of controlled experiments and numerical simulations.

The analysis will involve systematically varying the O-ring hardness, with hardness values obtained from experimental immersion tests serving as inputs in the simulation. The pressure will be applied to the hydraulic connection to mimic real-world conditions. This step aims to understand the effect of O-ring hardness under pressure on critical sealing attributes, particularly focusing on the contact force.

Mathematical relationships will be developed to quantify the trends in contact force (F_{axial}) and guide the selection of optimal O-ring hardness for enhanced sealing performance. The simulations will explore how varying levels of O-ring hardness influence the contact force, providing valuable insights into the material's response to pressure and aiding in the identification of the most suitable hardness for the given hydraulic connection. This analysis is crucial for achieving an optimized and robust sealing solution for gasoline injectors.

3. RESULTS AND DISCUSSIONS

Test and analysis setup as presented in methodology section was built and analyses were conducted. Based on obtained results, examinations and deductions are made in this section.

3.1. Media Immersion and Impact on O-ring

Before O-rings were put in medias as described in Section 2.2.2, dimensional and IRHD measurements were taken as shown in Table 3.1. After the test was carried out, measurements were taken again and values in Table 3.2 are retrieved.

Table 3.1 Initially Measured Dimensions and Hardness on O-rings

Media	No	Inner Diameter [mm]	Cross Section Diameter [mm]	Hardness [IRHD]
E100	1	4.450	3.024	85
	2	4.470	2.992	84
	3	4.417	3.031	85
	4	4.438	3.046	85
	5	4.452	3.010	85
E30	6	4.437	3.001	85
	7	4.501	2.978	84
	8	4.480	2.990	85
	9	4.464	3.014	86
	10	4.466	2.992	85
E85	11	4.483	2.982	84
	12	4.466	2.984	84
	13	4.531	2.956	86
	14	4.502	2.983	84
	15	4.413	3.034	85
E100	16	4.495	2.995	84
	17	4.488	2.968	85
	18	4.455	3.008	86
	19	4.491	2.975	85
	20	4.455	3.015	86
No media	21	4.458	3.018	85
	22	4.453	3.015	85
	23	4.464	3.015	85
	24	4.439	2.998	85
	25	4.486	2.984	85

Table 3.2 Measured Dimensions and Hardness on O-rings After Immersion

Media	**No**	**Inner Diameter [mm]**	**Cross Section Diameter [mm]**	**Hardness [IRHD]**
E100	1	4.466	3.034	86
	2	4.461	3.022	86
	3	4.468	3.007	86
	4	4.441	3.020	84
	5	4.480	2.990	84
E30	6	4.519	2.970	85
	7	4.466	3.030	85
	8	4.457	2.995	84
	9	4.476	3.015	85
	10	4.480	2.987	85
E85	11	4.549	2.953	85
	12	4.510	2.973	85
	13	4.478	2.982	84
	14	4.427	3.034	86
	15	4.502	2.988	85
E100	16	4.497	2.997	84
	17	4.466	3.014	85
	18	4.491	2.970	84
	19	4.509	2.969	83
	20	4.479	2.998	85

Even though the dimensions were measured, the comparison of change should be done on the volume instead of single dimensions. Thus, Equation (2.10) is used to calculate the volumes. The change in volumes is presented in percentages as shown in Figure 3.1.

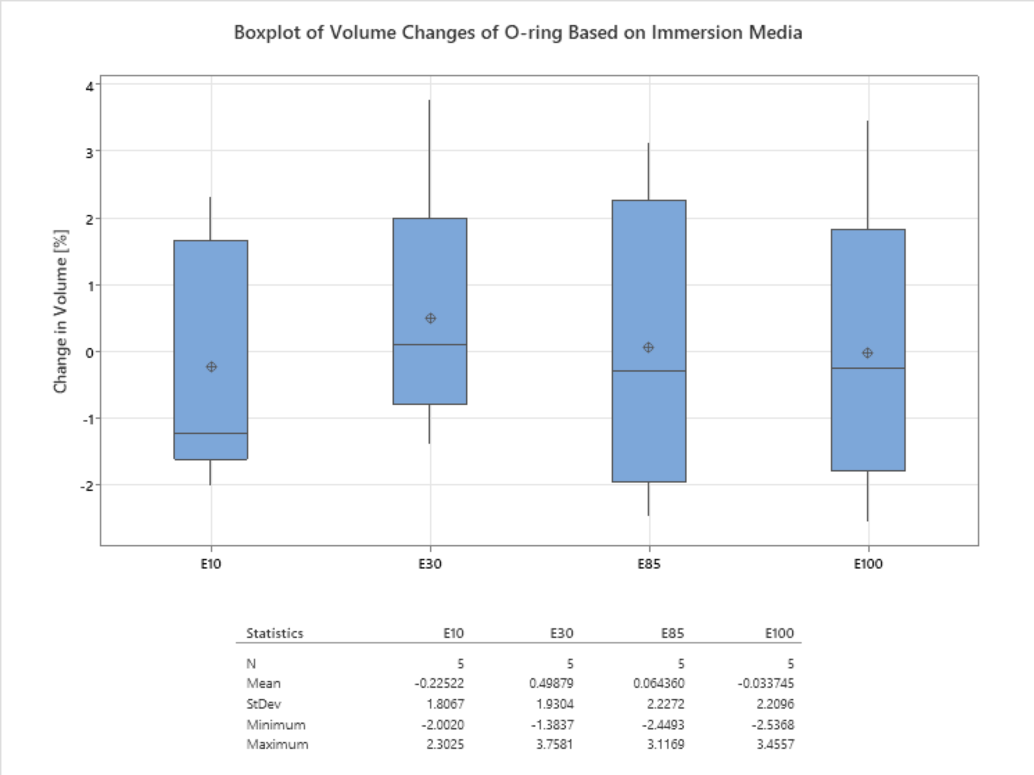

Figure 3.1 Volume Change of O-Rings Tested in Immersion Test

By evaluating the dimensional results shown in Table 3.1 and Table 3.2 no direct correlation between volume change and immersion media can be driven. Since there are many factors contributing to the results of dimensional measurements (e.g., human, machine calibration, environment) and readings are done in single microns, trend of volume change cannot be obtained.

However, VW's TL52666 norm defines mass percentage change on FKM O-rings as -3% to +1% for FAM B, and -2% to +1% for E85 immersion [37]. If it is assumed that the absorbed fuel in the O-ring vaporizes in drying and no media remains in the O-ring, then the mass change can be directly a reflection of volume change. Based on this assumption, E85 volumetric swelling result can be crosschecked with TL52666 norm. The test data presents values in thousandth digit, whereas VW TL52666 presents them in ones. For a rough comparison, test results are rounded to next tenth digit The maximum and minimum values is found to be -2.5% and +3.2%. When these are taken as borders, comparison of border limits can be shown in shown.

Table 3.3 Volumetric Change Limit Comparison for E85 Immersion

Data From	Lower Limit	Upper Limit
VW TL52666	-2%	+1%
Test Results	-2.5%	+3.2%

The difference between results comes from the test method. VW TL52666 follows the rules from DIN ISO 1817. Nevertheless, since TL52666 states that change can be seen in either (+) or (-) direction, similar conclusion can also be made for obtained results. In that case, values presented in Table 3.4 can be defined for border limits for tested medias when the same methodology is used.

Table 3.4 Change in O-Ring Volume After Immersion Test

E10	E30	E85	E100
-2.1% to +2.4%	-1.4% to +3.8%	-2.5% to +3.2%	-2.6% to -3.5%

Hardness values before and after the test was presented in Table 3.1 and Table 3.2. If these values are evaluated in terms of change, the final IRHD value must be subtracted from the initial. Based on the minimum and maximum change values, limit for change can be derived as shown in Table 3.5.

Table 3.5 Change in O-ring IRHD After Immersion Test

E10	E30	E85	E100
-1 to +2	-1 to +1	-2 to +2	-2 to 0

To get a better understanding of mechanical performance change, tensile strength test was performed on O-rings after the immersion test. The test output is analyzed under strength and elongation values as shown in Figure 3.2 and Figure 3.3. Even though E10 immersion results are similar to non-immersed values, it is clearly seen that higher ethanol content lowers the mechanical performance of the O-ring. The result does not specifically mean that O-rings under higher ethanol content will fail in field operations, but it means that they are more likely to crack and fail.

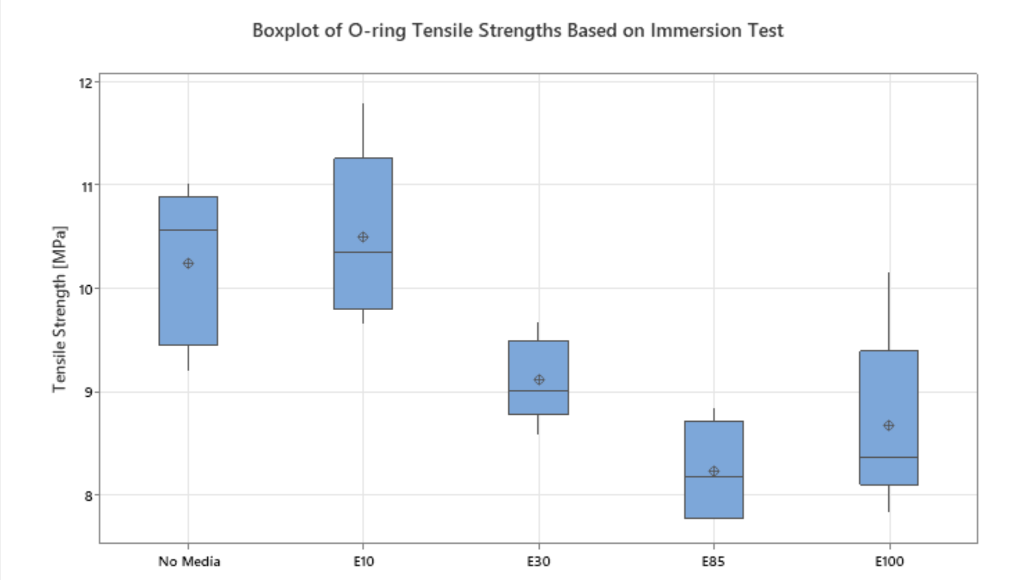

Statistics	No Media	E10	E30	E85	E100
N	5	5	5	5	5
Mean	10.244	10.490	9.1074	8.2301	8.6710
StDev	0.76238	0.82902	0.40677	0.47695	0.87899
Minimum	9.1968	9.6540	8.5908	7.7687	7.8370
Maximum	11.009	11.790	9.6756	8.8405	10.157

Figure 3.2 Boxplot of O-ring Tensile Strength

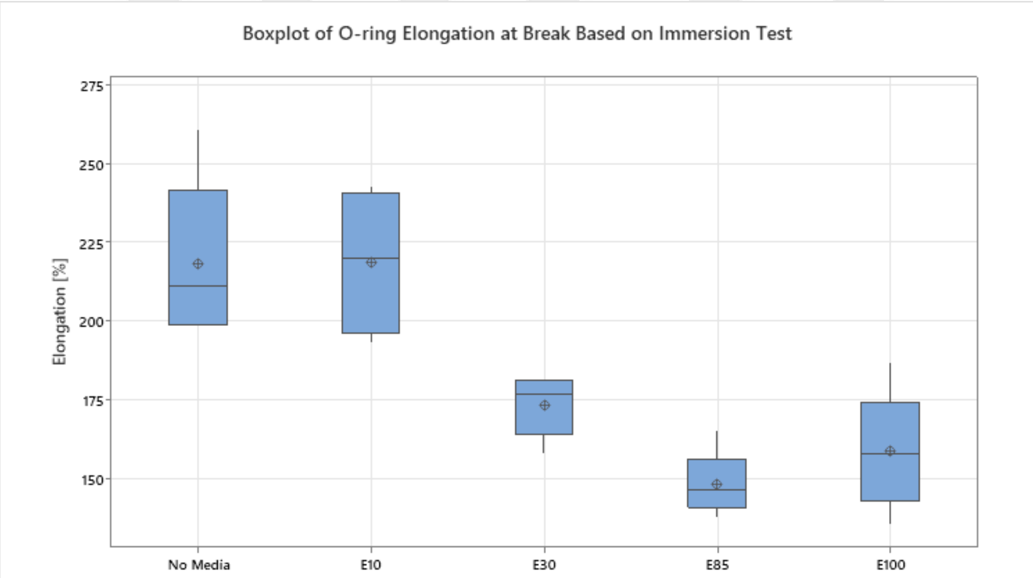

Statistics	No Media	E10	E30	E85	E100
N	5	5	5	5	5
Mean	218.30	218.76	173.43	148.31	158.66
StDev	25.620	22.284	9.7133	10.135	18.710
Minimum	198.56	193.11	158.06	138.05	135.91
Maximum	260.73	242.54	181.20	165.17	186.99

Figure 3.3 Boxplot of O-ring Elongation at Break Values

3.2. Numerical Analysis

First starting point for numerical analysis was to investigate effect of O-rings inner diameter change. To get starting and end dimensions, corresponding dimensions for when compression equals to 10% and 30% was calculated via Equation (2.8). Found values were minimum and maximum dimensions were 3.746 mm and 5.816 mm, respectively. However, inner diameter cannot be bigger than the bore diameter. Thus, the maximum dimension for analysis was chosen as 4.6 mm. In addition, ISO 3601-01 norm suggest O-ring dimension with tenth digits. Hence, step size for numerical analysis was chosen as 0.01; and start point was determined as 3.74 mm, whereas end point was chosen as 4.60 mm. Based on this input, compression, groove fill and initial stretch values were calculated (see Figure 3.4).

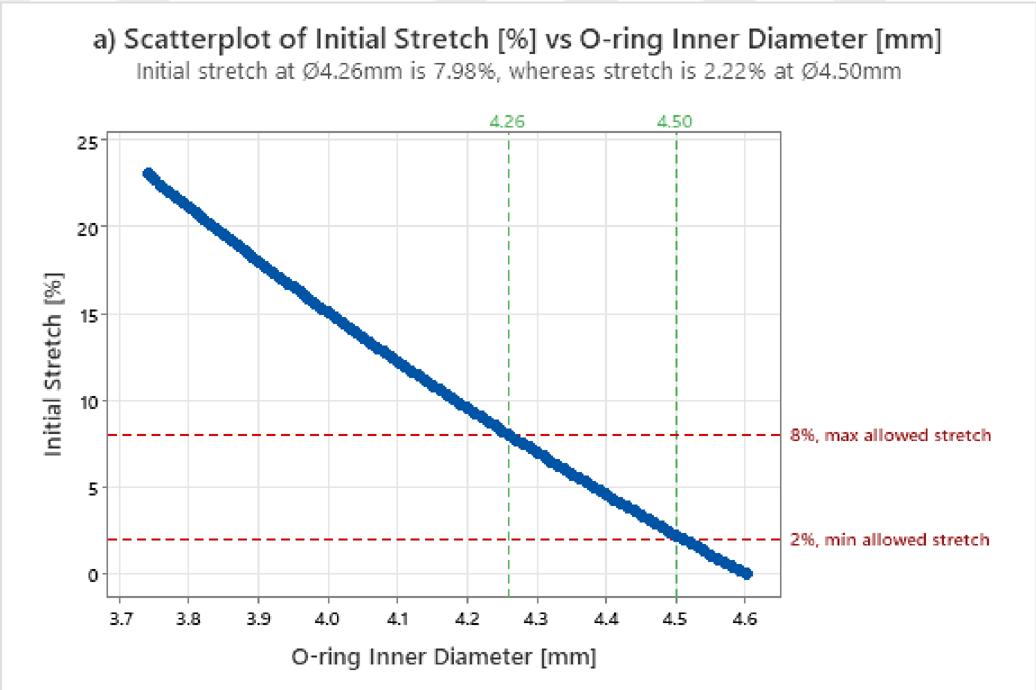

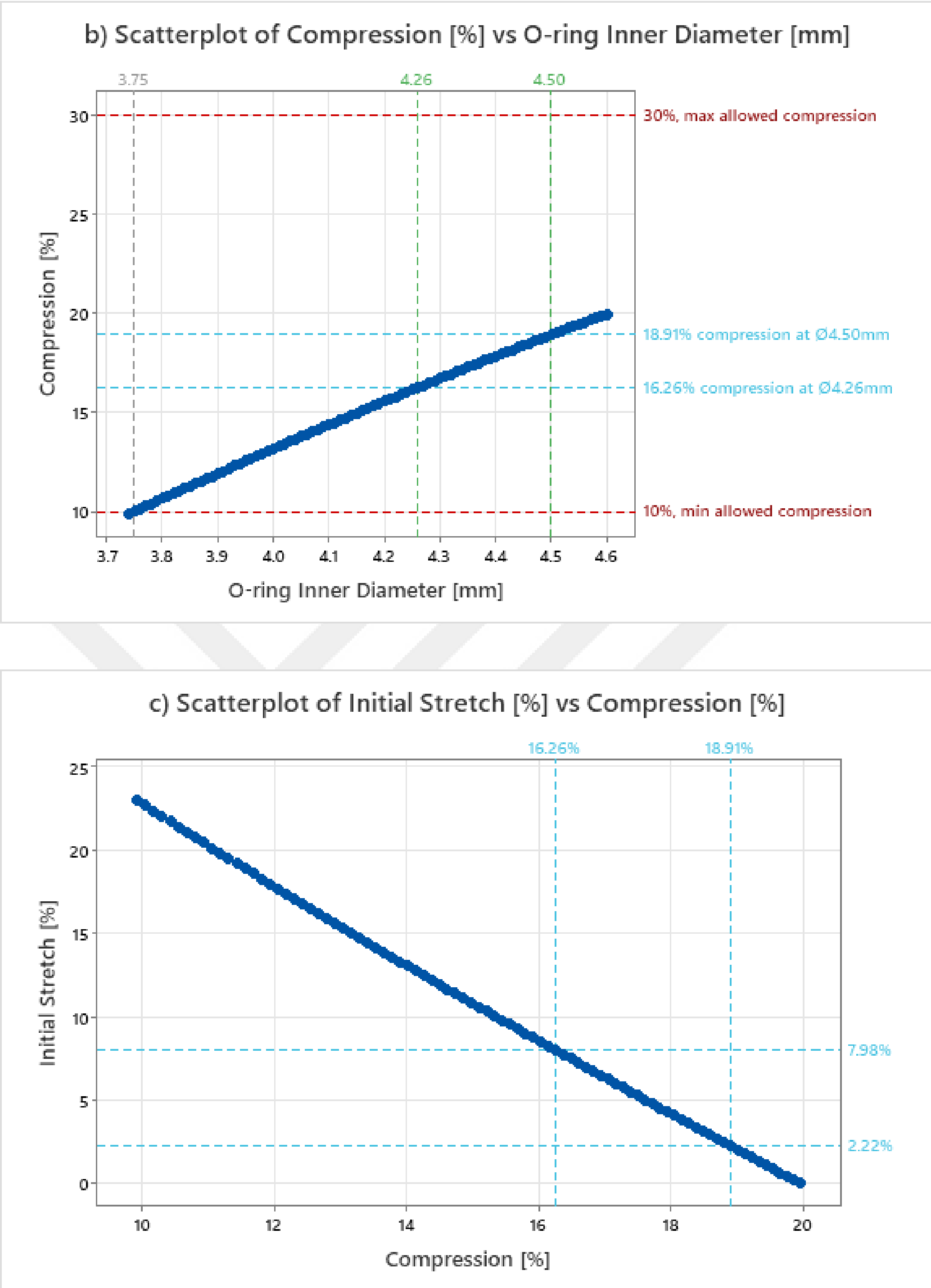

Figure 3.4 Effect of O-ring's Inner Diameter on a) Initial Stretch, b) Compression, c) Initial Stretch and Compression

When the initial stretch is calculated via Equation (2.5), Figure 3.4a is obtained. Based on the stretch limits, dimension of inner diameter is acceptable from 4.26 mm to 4.50 mm. Compression values as shown in Figure 3.4b shows that all evaluated values are within the borders except 3.74 mm. Out of all inputs, every single one them had fell under the maximum groove fill; thus, groove fill was not a determining factor here. As a combination of both initial stretch and compression, Figure 3.4c, results found in the initial stretch provides a stricter gap for O-ring inner diameter. Hence, borders for inner diameter are defined upon initial stretch output.

Independently from inner diameter numerical study, cross sectional diameter was also investigated. Similarly, compression values were calculated and from 2.72 mm to 3.50 mm with increment of 0.01 mm was used as input for the analysis. Since cross section diameter does not have contribution to initial stretch, stretch values were not calculated.

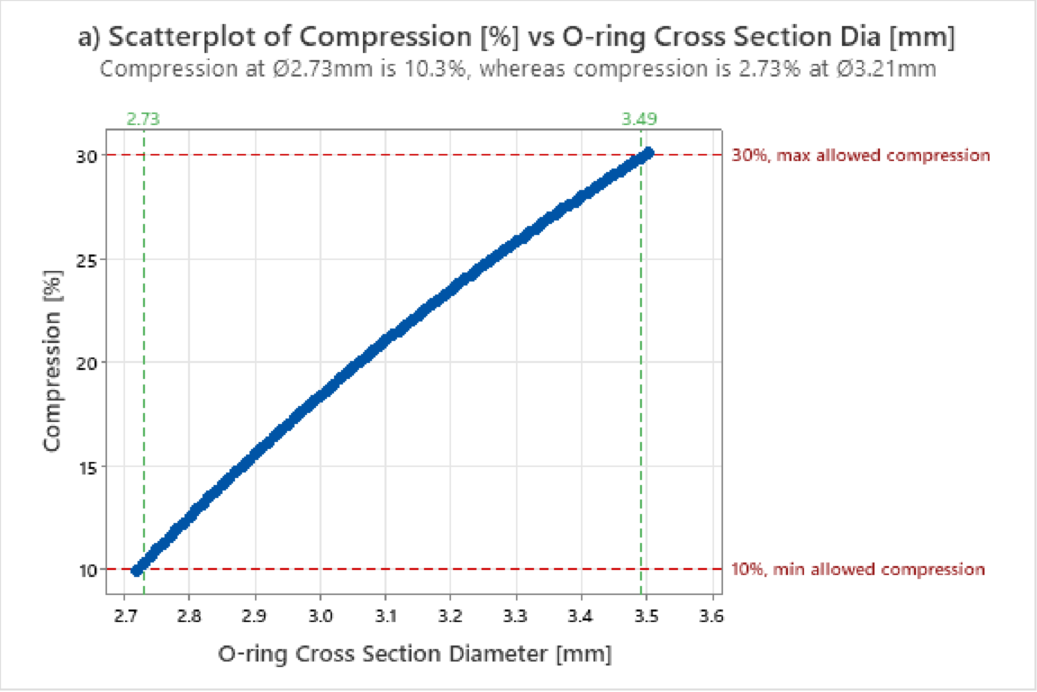

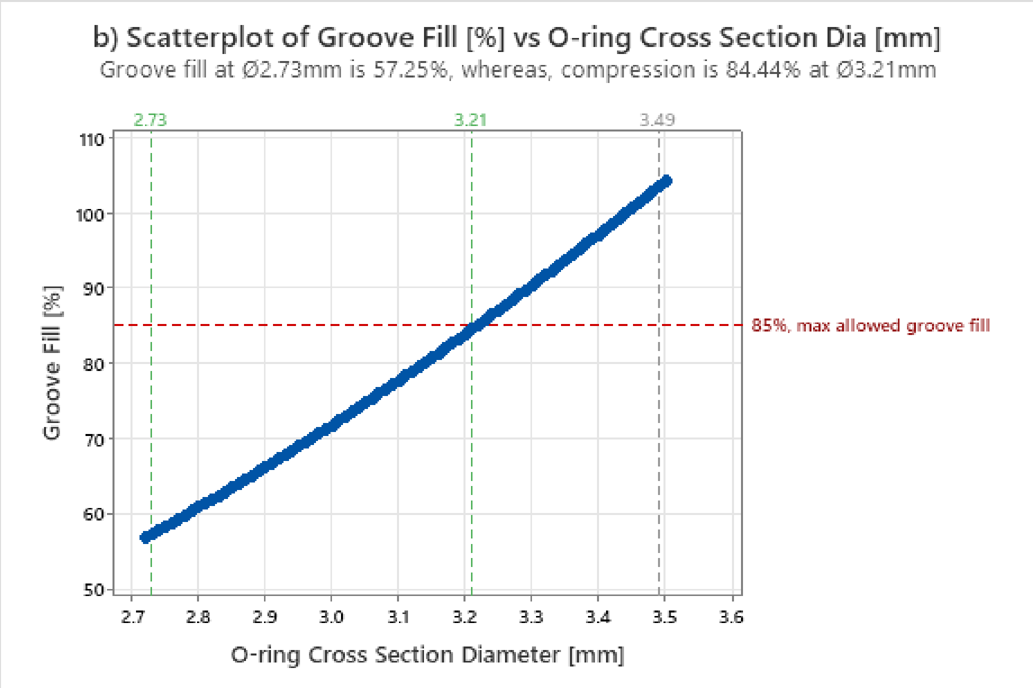

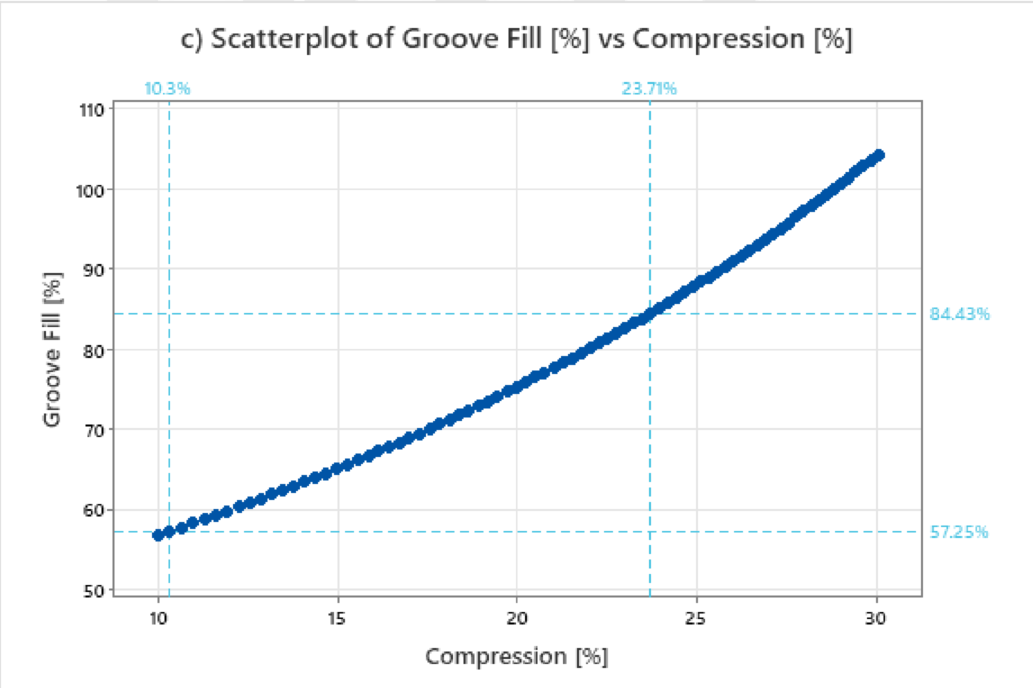

Figure 3.5 Effect of O-ring's Cross Section Diameter On a) Compression, b) Groove Fill, c) Compression and Groove Fill

Upon Figure 3.5a, 2.73mm and 3.49 mm diameters were the limit that satisfies compression requirements. However, Figure 3.5b has proven that maximum cross section diameter can be 3.21 mm, due to maximum groove fill requirement. As a result, diameter from 2.73 mm to 3.29 mm could be acceptable in this case.

The last independent study conducted was on piston diameter. By calculating the border limits and rounding them up, start and end dimensions were set as 4.46 mm to 5.77 mm and Figure 3.6 was obtained. Based on the results, only dimensions in between 4.54 mm and 4.80 mm meets the requirements.

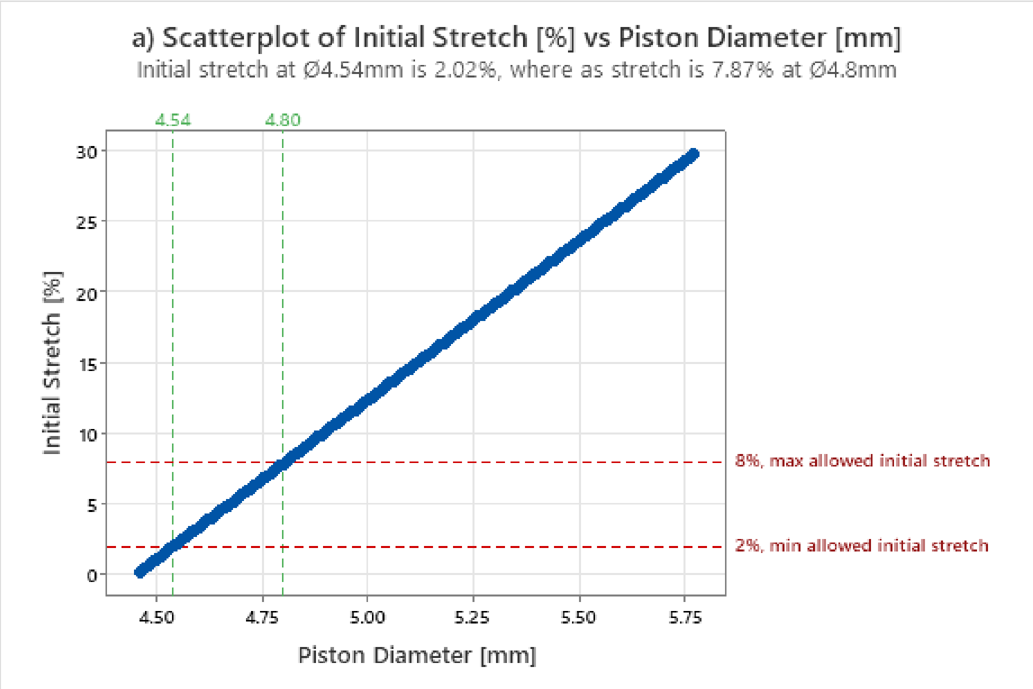

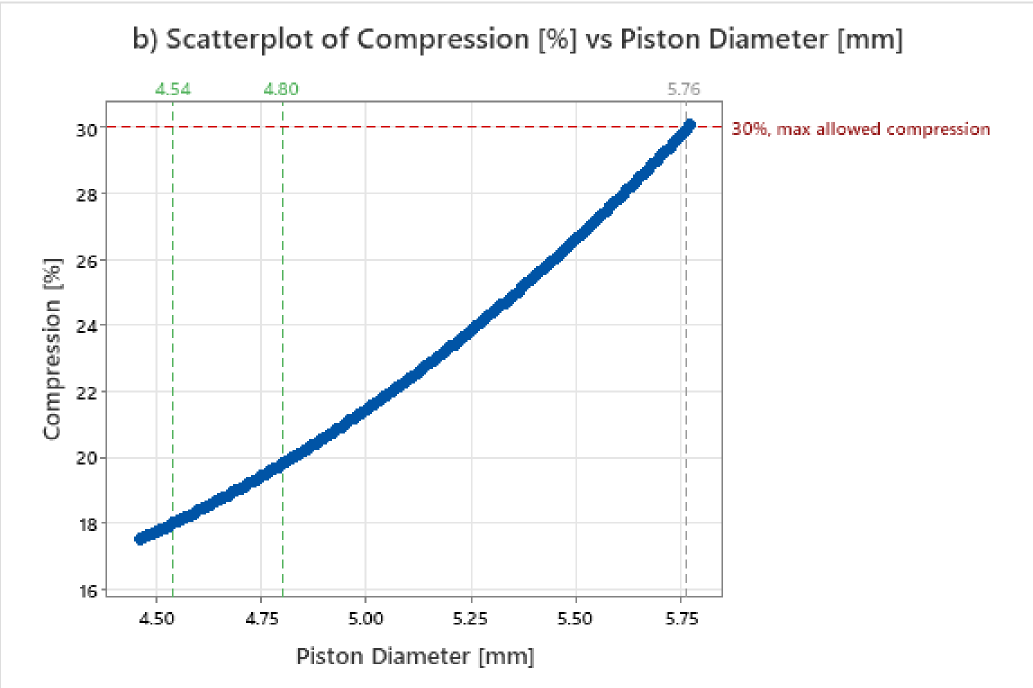

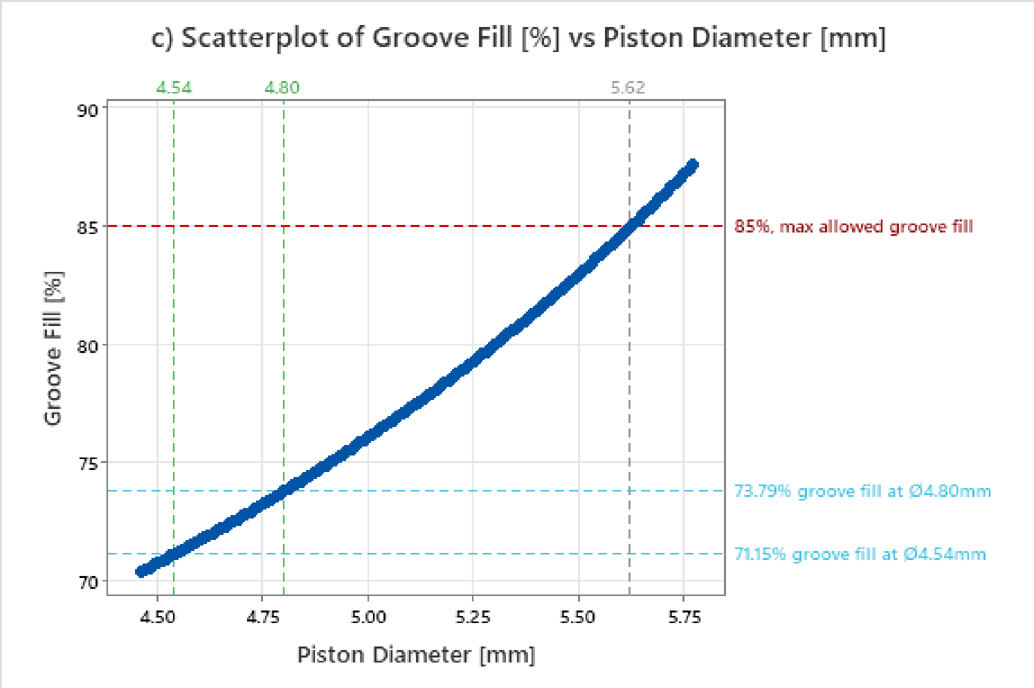

Figure 3.6 Effect of Piston Diameter On a) Initial Stretch, b) Compression, c) Groove Fill

Figure 3.4, Figure 3.5 and Figure 3.6 shows the behavior of dimension on under various conditions. However, to evaluate the contribution of these dimensions, they must be observed under same conditions. All 3 dimensions have effect on compression and groove fills; thus, they can be compared to each other on these terms. In order to compare the results, only upper and lower limit of dimensions that satisfy design concept was used and Figure 3.7 developed.

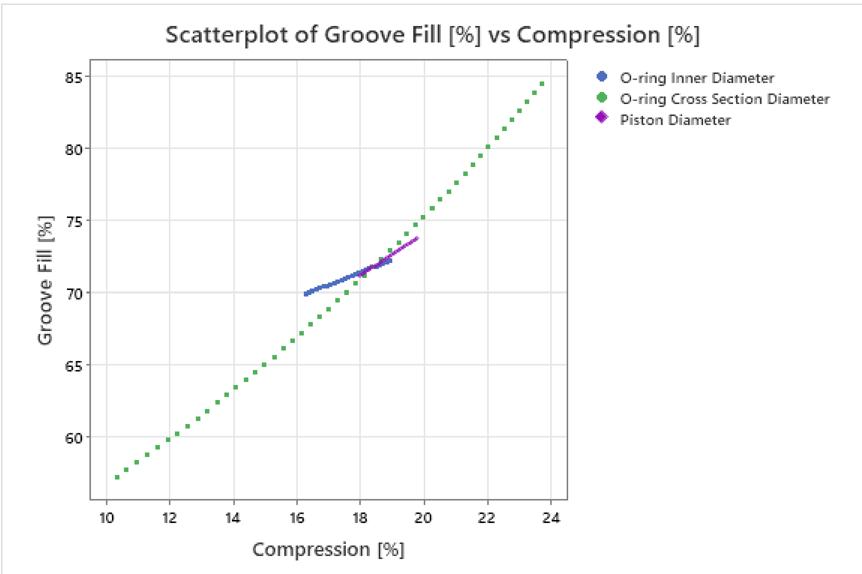

Figure 3.7 Comparison of Dimension Contribution to Sealing Properties

It can be derived from Figure 3.7 that increment of O-ring cross section effects the overall compression and groove fill much higher than the other two. The comparison should also include the force and pressure effects as well however, the elastic modulus specific to the material had to be found. To find this, non-immersed results found in Figure 3.2 was converted to stress vs. strain curve and elastic modulus at 100% elongation was calculated according to (3.1)) and Figure 3.8. The average elastic modulus at 100% elongation was found to be 6.17Mpa.

$$\sigma = \varepsilon E_{100\%} \tag{3.1}$$

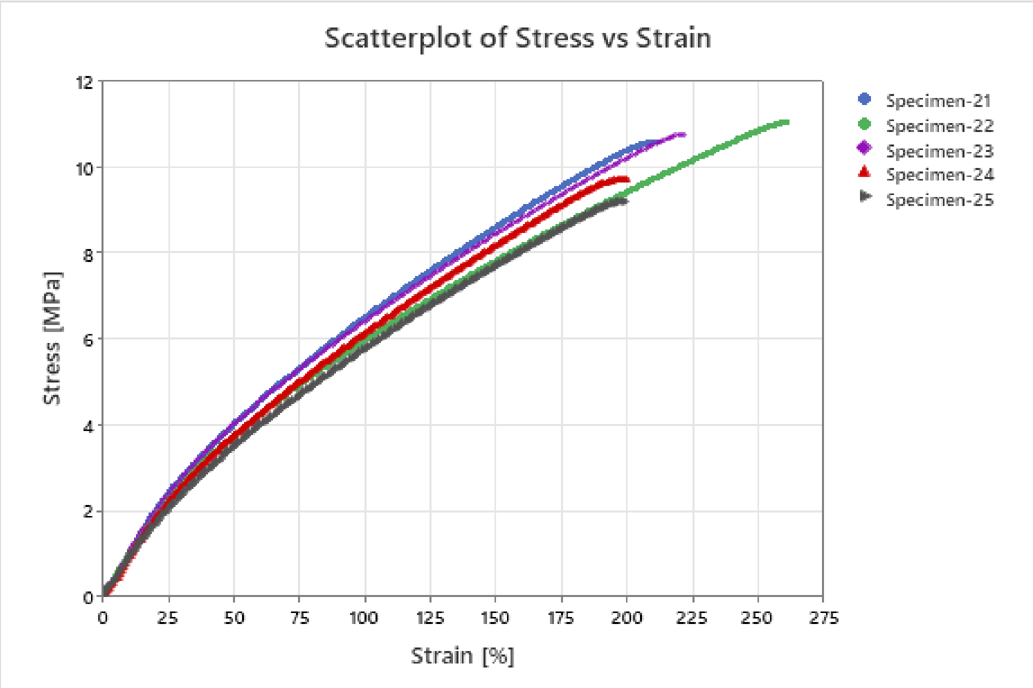

Figure 3.8 Stress vs Strain of Non-immersed O-rings

To compare the force and pressure based on parameters, the dimensional values that meet the design expectations were used. The force and pressure values were calculated with the found elastic modulus, it was observed that scattering in O-ring cross section parameter becomes higher and the values extend further compared to other two parameters. In addition, the grey reference line in Figure 3.9 represents the condition of actual HDEV6 O-ring as a reference. This shows that there is a possibility to improve the current design.

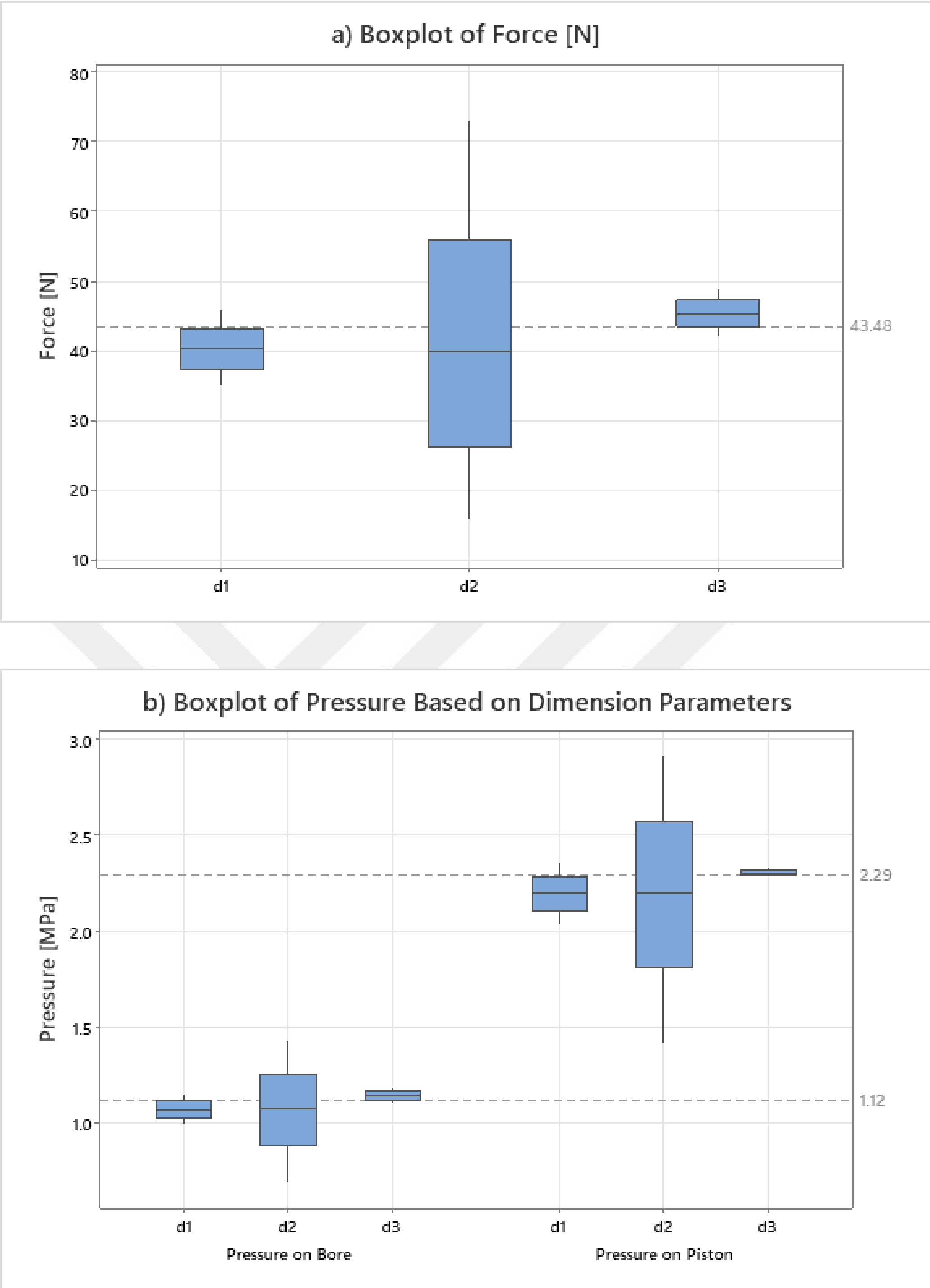

Figure 3.9 Force and Pressure Comparison of Parametric Dimensions

As up to this point, O-rings inner diameter, cross-section and piston diameter variations had been analyzed and effects on the sealing design was investigated. However, dependent analysis was not conducted, meaning that combination of found border dimensions were not created and its outcome was not investigated.

Based on 3 inputs (d_1, d_2, d_3), combinations were created. With the found combinations, figures below were obtained.

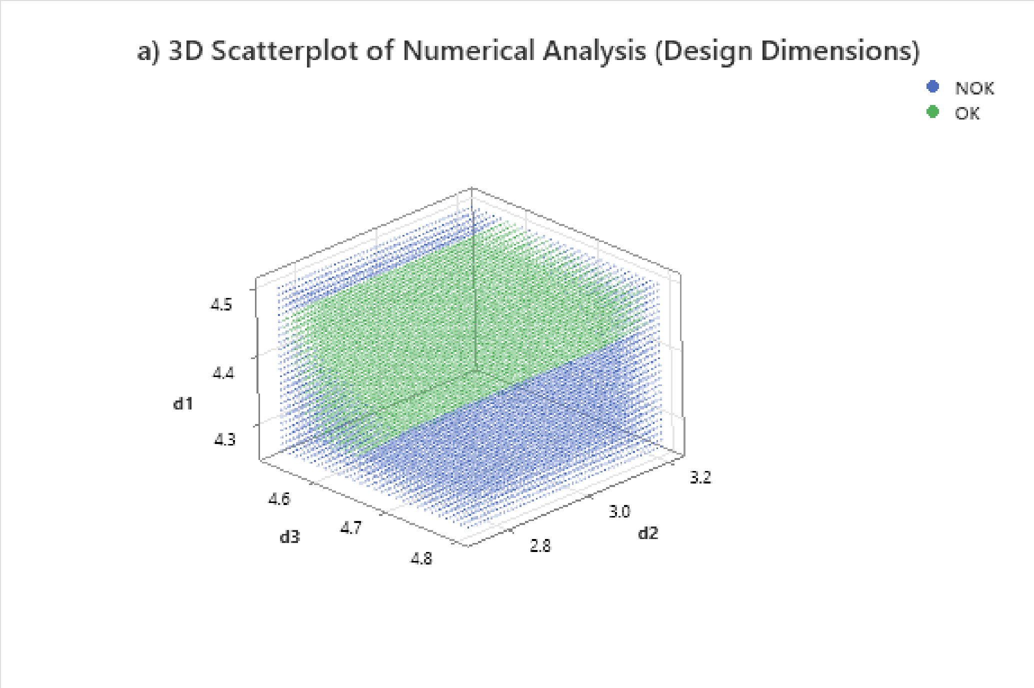

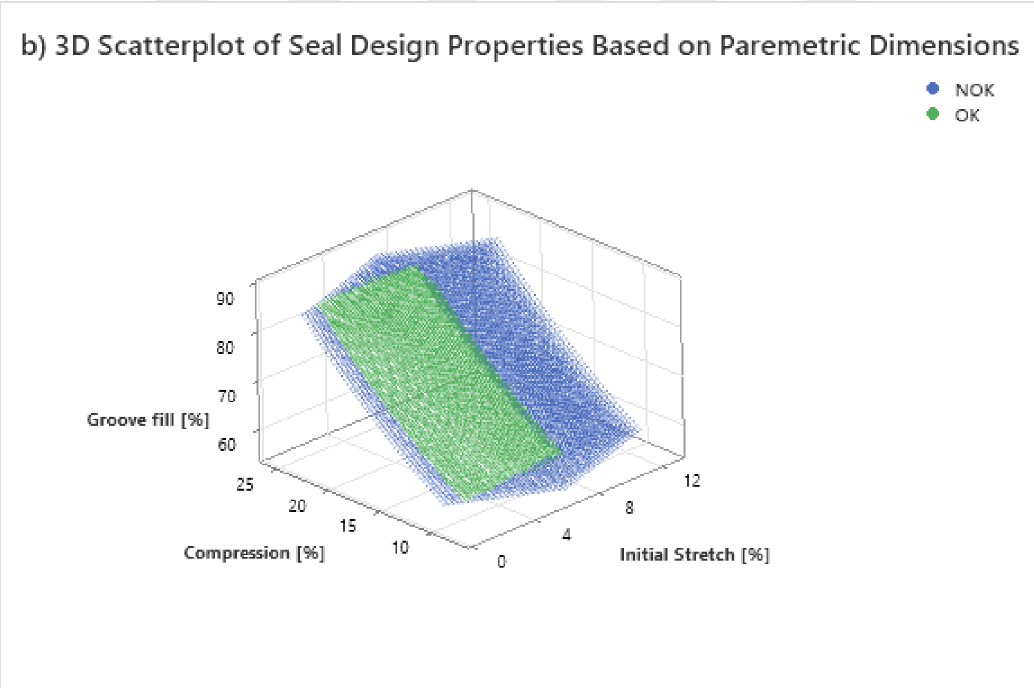

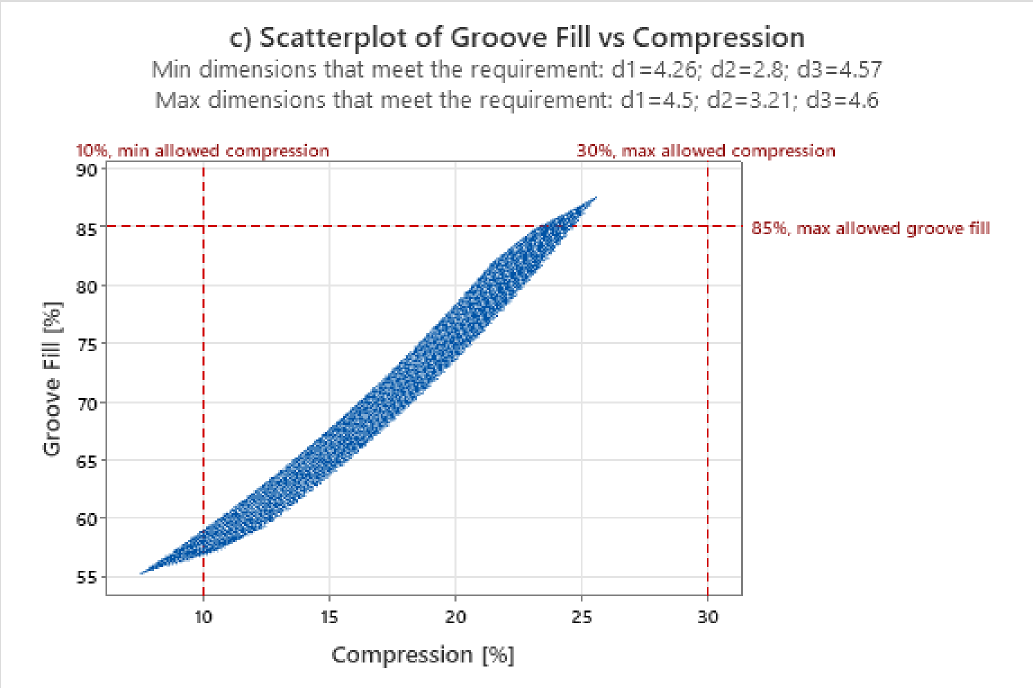

Figure 3.10 Combined Analysis a) Dimensions, b) Seal Design Properties, c) Groove Fill and Compression Relation

Results had proven that out of all combinations the minimum dimension can be 4.26 mm for inner diameter, 2.8 mm for cross section and 4.57 mm for piston diameter; whereas max dimensions can be 4.45 mm inner diameter, 3.21 mm for cross section and 4.6 mm for piston diameter.

Contact force and pressure for these values are presented in Figure 3.6.

Table 3.6 Acting Force and Pressure on Min and Max Dimensions

d1 [mm]	d2 [mm]	d3 [mm]	F [N]	Pressure on Bore [MPa]	Pressure on Piston [MPa]
4.26	2.80	4.57	15.30	0.67	1.38
4.50	3.21	4.60	76.29	1.46	2.98

The values can be interpreted for O-rings when they are not subjected to fuels. Since fuel deteriorates the integrity of O-ring and it becomes softer, the elastic modulus tends to increase. To visualize this behavior, elastic modulus of O-ring when subjected to gasoline-ethanol blends were retrieved based on the results retrieved in Figure 3.2 and Figure 3.3.

Table 3.7 Elastic Modulus at 100% Elongation of O-rings After Immersion

Blend	E10	E30	E85	E100
Elastic Modulus [Mpa]	6.22	6.52	6.76	6.67

Table 3.8 Comparison of Immersed O-rings Properties

Blend	**Property**	**d1; d2; d3**		
		4.26; 2.8; 4.57	**4.45; 3; 4.6**	**4.50; 3.21; 4.6**
Non-immersed	Force [N]	15.30	43.48	76.29
	Pressure on Bore [MPa]	0.67	1.12	1.46
	Pressure on Piston [MPa]	1.38	2.29	2.98
E10	Force [N]	15.41	43.81	76.87
	Pressure on Bore [MPa]	0.68	1.13	1.47
	Pressure on Piston [MPa]	1.39	2.31	3.01
E30	Force [N]	16.15	45.92	80.57
	Pressure on Bore [MPa]	0.71	1.18	1.54
	Pressure on Piston [MPa]	1.46	2.42	3.15
E85	Force [N]	16.76	47.64	83.58
	Pressure on Bore [MPa]	0.73	1.23	1.60
	Pressure on Piston [MPa]	1.51	2.51	3.27
E100	Force [N]	16.52	46.97	82.41
	Pressure on Bore [MPa]	0.72	1.21	1.58
	Pressure on Piston [MPa]	1.49	2.47	3.22

What can be observed from this table is that softening of the O-ring provides better sealing properties. Force and pressure values increase even though the material softens over time. O-ring with the biggest dimension provides the best sealing. In addition to that, when 100% biofuel-ethanol is used in the vehicle, biggest dimensioned O-ring's tendency to apply force on its surroundings increases by 7.6%. Moreover, the pressure applied on the bore increases by 8.2% and pressure on piston increases by 20%.

4. CONCLUSION

In conclusion, this thesis aimed to explore how O-rings behave in gasoline injection systems when exposed to different gasoline blends, with a specific focus on improving the hydraulic connection between the injector and rail. The introduction emphasized the vital role of O-rings in sealing hydraulic connections, especially in various types of gasoline injection systems. It also highlighted the impact of different gasoline blends on the mechanical properties of O-rings and explained the importance of optimizing the hydraulic connection.

The methodology used a two-fold approach, employing media immersion tests to check for volume swelling and numerical analysis to enhance O-ring dimensions and piston parameters. This comprehensive method aimed to provide a thorough understanding of O-ring behavior, considering both material characteristics and geometric factors.

The results, presented through graphs and tables, showed no direct link between ethanol content in gasoline blends and O-ring deterioration. However, a notable observation was made – higher ethanol concentrations were linked to a decline in O-ring performance. This nuanced insight emphasizes the complex relationship between O-ring material and various gasoline compositions.

By optimizing dimensions, a substantial 30% increase in O-ring contact pressures can be achieved, ultimately enhancing the sealing function. Additionally, the study revealed that higher ethanol content, particularly in the form of 100% ethanol-biofuel, not only softens the material but also notably augments the sealing behavior, with an increase of 8.2% and 20% in contact pressure on the bore and piston respectively. These findings underscore the potential for targeted improvements in hydraulic sealing efficiency through careful dimension optimization and consideration of ethanol content, offering valuable insights for enhancing system performance and durability.

In the broader context of fuel system design, these findings offer valuable perspectives for developing resilient O-ring components. The absence of a straightforward correlation highlights the need for a nuanced understanding of the intricate connections between O-ring performance and fuel composition. This study lays the groundwork for future research aimed at improving hydraulic connections and strengthening the endurance of O-rings in gasoline injection systems.

Furthermore, it is anticipated that the ECHA's PFAS restriction, expected to be effective in 2026/2027, may necessitate material updates in FKM O-rings [38]. Should this regulation come into effect, the findings of this study could serve as potential references for upcoming material development activities. The knowledge gained from this thesis is poised to make meaningful contributions to the automotive industry by guiding advancements in fuel system technology and enhancing the overall efficiency and reliability of internal combustion engines.

REFERENCES

[1] S. Pischinger, "Current and Future Challenges for Automotive Catalysis: Engine Technology Trends and Their Impact," *Topics in Catalysis*, vol. 59, pp. 834-844, May 2016.

[2] R. J. Hames, D. F. Merrion and H. S. Ford, "Some Effects of Fuel Injection System Parameters on Diesel Exhaust Emissions," in *SAE Technical Paper Series*, 1971.

[3] A. Marchuk, V. Likhanov and O. Lopatin, "Alternative energy: methanol, ethanol and alcohol esters of rapeseed oil as eco-friendly biofuel," *Theoretical and Applied Ecology*, pp. 80-86, 2019.

[4] A. K. Agarwal, A. P. Sing, T. Gupta, R. A. Agarwal, N. Sharma, S. K. Pandey and B. Ateeq, "Toxicity of exhaust particulates and gaseous emissions from gasohol (ethanol blended gasoline)-fuelled spark ignition engines," *Environ. Science: Processes & Impacts*, vol. 22, no. 7, pp. 1540-1553, 2020.

[5] S. Padala, M. K. Le, S. Kook and E. R. Hawkes, "Imaging diagnostics of ethanol port fuel injection sprays for automobile engine applications," *Applied Thermal Engineering*, pp. 24-37, April 2013.

[6] M. Koç, Y. Sekmen, T. Topgül and H. S. Yücesu, "The effects of ethanol–unleaded gasoline blends on engine performance and exhaust emissions in a spark-ignition engine," *Renewable Energy*, vol. 34, no. 10, pp. 2101-2106, October 2009.

[7] A. K. Agarwal, "Biofuels (alcohols and biodiesel) applications as fuels for internal combustion engines," *Progress in Energy and Combustion Science*, vol. 33, pp. 233-271, June 2007.

[8] T. Dhawale, A. Chougule and V. Ware, "Implementation of AI for Injector Quality Inspection," *International Journal of Scientific Research in Computer Science, Engineering and Information Technology*, pp. 21-26, 2022.

[9] M. Melaina and J. Bremson, "Refueling availability for alternative fuel vehicle markets: Sufficient urban station coverage," *Energy Policy,* vol. 36, pp. 3233-3241, August 2008.

[10] A. Calam, H. Solmaz, A. Uyumaz, S. Polat, E. Yılmaz and Y. İçingür, "Investigation of usability of the fusel oil in a single cylinder spark ignition engine," *Journal of the Energy Institute,* pp. 258-265, August 2015.

[11] J. Tibaquirá, J. Huertas, S. Ospina, L. Quirama and J. Niño, "The Effect of Using Ethanol-Gasoline Blends on the Mechanical, Energy and Environmental Performance of In-Use Vehicles," *Energies,* p. 221, 2018.

[12] W. Hentschel, "Optical diagnostics for combustion process development of direct-injection gasoline engines," *Proceedings of the Combustion Institute,* vol. 28, no. 1, pp. 1119-1135, 2000.

[13] F. Zhao, M. -C. Lai and D. L. Harrington, "Automotive spark-ignited direct-injection gasoline engines," *Progress in Energy and Combustion Science,* vol. 25, pp. 437-532, October 1999.

[14] S. Y. Lee, H. J. Lee, Y. T. Kang and J. T. Chung, "Effects of injection strategies on the flow and fuel behavior characteristics in port dual injection engine," *Energy,* vol. 165, pp. 666-676, 2018.

[15] T. D. Spegar, "Minimizing Gasoline Direct Injection (GDi) Fuel System Pressure Pulsations by Robust Fuel Rail Design," 2011.

[16] G. Saliba, R. Saleh, Y. Zhao , A. A. Presto, A. T. Lambe, B. Frodin, S. Sardar, H. Maldonado , C. Maddox, A. A. May, G. T. Drozd, A. H. Goldstein, L. M. Russell, F. Hagen and A. L. Robinson, "Comparison of Gasoline Direct-Injection (GDI) and Port Fuel Injection (PFI) Vehicle Emissions: Emission Certification Standards, Cold-Start, Secondary Organic Aerosol Formation Potential, and Potential Climate Impacts," *Environmental Science & Technology,* pp. 6542-6552, April 2017.

[17] K. Hashimoto, A. Maeda, K. Hosoya and Y. Todani, "Specialty Elastomers for Automotive Applications," *Rubber Chemistry and Technology,* vol. 71, pp. 449-519, July 1998.

[18] TRP Polymer Solutions, "FKM Chemical Structure: FKM Material Properties," June 2020. [Online]. Available: https://trp.co.uk/fkm-chemical-structure/.

[19] E. W. Thomas, "Fluoroelastomer Compatibility with Bioalcohol Fuels," *SAE International Journal of Fuels and Lubricants,* p. 462–473, April 2009.

[20] R. C. Klingender, Handbook of Specialty Elastomers, CRC Press, 2008.

[21] R. Rudbahs and R. Smigins, "Experimental research on biodiesel compatibility with fuel system elastomers," *Engineering for Rural Development,* vol. 13, pp. 278-282, 2014.

[22] M. Kass, C. Janke, S. Pawel, J. Thomson, I. H. Meyer and T. Theiss, "Compatibility study for plastic, elastomeric, and metallic fueling infrastructure materials exposed to aggressive formulations of isobutanol-blended gasoline," Office of Scientific and Technical Information (OSTI), United States, 2013.

[23] J. Yamabe, A. Koga and S. Nishimura, "Failure behavior of rubber O-ring under cyclic exposure to high-pressure hydrogen gas," *Engineering Failure Analysis,* vol. 35, pp. 193-205, December 2013.

[24] Z. Li, "Study on the Sealing Performance of O-ring under High-Pressure Environment," *Journal of Physics: Conference Series,* vol. 2419, January 2023.

[25] C. Sayın, M. K. Balki and S. Erdoğan, Yakıtlar ve Yanma, Nobel Akademi, 2021.

[26] International Organization for Standardization, *Rubber, vulcanized or thermoplastic — Determination of the effect of liquids,* ISO, 2022.

[27] Vötsch Industrietechnik, "Temperature Shock Test Chambers: Systems for Extreme Temperature Cycling," 2023.

[28] EMCO-TEST Prüfmaschinen GmbH, "Shore Test," 2023. [Online]. Available: https://www.emcotest.com/en/the-world-of-hardness-testing/hardness-know-how/theory-of-hardness-testing/other-test-procedures/shore-test/. [Accessed 6 February 2023].

[29] International Organization for Standardization, *Rubber, vulcanized or thermoplastic: Determination of hardness,* ISO, 2018.

[30] B. N. A. Inc., "IRHD Compact III – Automatic Hardness Tester," Bareiss, [Online]. Available: https://www.bareiss-testing.com/product/automatic-compact-irhd-tester-irhd-compact-iii/. [Accessed 21 December 2023].

[31] Zwick Roell, *Product Information: Materials Testing Machines zwickiLine Z0.5 to Z5.0,* Zwick Roell.

[32] International Organization for Standardization, *Fluid power systems - O-rings - Part 1: Inside diameters, cross-sections, tolerances and designation codes,* 2012.

[33] International Organization for Standardization, *Fluid power systems — O-rings — Part 2: Housing dimensions for general applications,* 2016.

[34] Trelleborg Sealing Solutions, *O-Rings and Back-up Rings,* 2013.

[35] P. B. Lindley, "Load-Compression Relationships of Rubber Units," *Jour. of Strain Analysis,* vol. 1, pp. 190-195, 1966.

[36] P. B. Lindley, "Compression Characteristics of Laterally Unrestrained Rubber O-ring," *Jour. Inter. Rubber Inst.,* vol. 1, pp. 202-2013, 1967.

[37] Volkswagen AG, *FKM-Elastomer für Ottokraftstoff-Einsätze bei Hochdruckinjektionssystemen - Werkstoffanforderungen,* 2017.

[38] ECHA (European Chemicals Agency), "ANNEX XV RESTRICTION REPORT – Per- and polyfluoroalkyl substances (PFASs)," 2023.

RÉSUMÉ

He graduated as a Mechanical Engineer from Ozyegin University in 2020, having entered on a full scholarship in 2015. During his undergraduate years, he actively contributed to various academic and research projects, focusing on areas relevant to the automotive industry, while also maintaining a position on the Ozyegin University Honor List throughout his journey. In 2020, he presented a paper titled "Rapid Heating and Cooling Chamber for A Photonics Junction Measurement System" at the IEEE ITherm Virtual Conference, demonstrating his expertise in automotive engineering and thermal management systems. Since 2021, he has been contributing his skills and knowledge as a Research and Development Engineer in the automotive industry. His dedication and proficiency led to his promotion to Senior Engineer in 2023. Continuing his academic journey, he is currently pursuing postgraduate studies at the Marmara University Institute of Science, further specializing in automotive engineering.